J Neurophysiol 112: 61–80, 2014.
First published November 20, 2013; doi:10.1152/jn.00505.2013.

Intentional signal in prefrontal cortex generalizes across different sensory modalities

Kyuwan Choi[1,2] and Elizabeth B. Torres[1,2,3]

[1]*Psychology Department, Rutgers University, Piscataway, New Jersey;* [2]*Center for Computational Biomedicine Imaging and Modeling, Computer Science Department, Rutgers University, Piscataway, New Jersey; and* [3]*Rutgers Center for Cognitive Science, Rutgers University, Piscataway, New Jersey*

Submitted 12 July 2013; accepted in final form 12 November 2013

Choi K, Torres EB. Intentional signal in prefrontal cortex generalizes across different sensory modalities. *J Neurophysiol* 112: 61–80, 2014. First published November 20, 2013; doi:10.1152/jn.00505.2013.—Biofeedback-EEG training to learn the mental control of an external device (e.g., a cursor on the screen) has been an important paradigm to attempt to understand the involvements of various areas of the brain in the volitional control and the modulation of intentional thought processes. Often the areas to adapt and to monitor progress are selected a priori. Less explored, however, has been the notion of automatically emerging activation in a particular area or subregions within that area recruited above and beyond the rest of the brain. Likewise, the notion of evoking such a signal as an amodal, abstract one remaining robust across different sensory modalities could afford some exploration. Here we develop a simple binary control task in the context of brain-computer interface (BCI) and use a Bayesian sparse probit classification algorithm to automatically uncover brain regional activity that maximizes task performance. We trained and tested 19 participants using the visual modality for instructions and feedback. Across training blocks we quantified coupling of the frontoparietal nodes and selective involvement of visual and auditory regions as a function of the real-time sensory feedback. The testing phase under both forms of sensory feedback revealed automatic recruitment of the prefrontal cortex with a parcellation of higher strength levels in Brodmann's areas 9, 10, and 11 significantly above those in other brain areas. We propose that the prefrontal signal may be a neural correlate of externally driven intended direction and discuss our results in the context of various aspects involved in the cognitive control of our thoughts.

brain computer interface; coadaptation; intentional control; prefrontal cortex; volitional control

SINCE ITS EARLY CONCEPTION (Vidal 1973) the brain-machine interface (BMI) or brain-computer interface (BCI) paradigm has gained tremendous popularity. Because of its success in developing algorithms and experimental settings that could aid paralyzed patients to use their brain signals to intentionally control directional motions of external devices, this early concept has become a booming field in neuroscience and bioengineering (among other representative work, Contreras-Vidal and Bradberry 2011; Contreras-Vidal et al. 2010; Lebedev and Nicolelis 2006; Millan Jdel et al. 2004; Wolpaw and McFarland 1994).

In recent years several lines of BMI/BCI research have focused on the harnessing of neural signals from specific brain areas to adapt in real time a map relating these signals to the states of the motion control of some external device (Carmena et al. 2003; Lebedev et al. 2005; Serruya et al. 2002; Taylor et al. 2002; Wessberg et al. 2000). The success of using the spike and/or the local field potential (LFP) signals for intentional control of external events has been widely recognized for different cortical regions in both human and nonhuman primates (Andersen et al. 2004; Hatsopoulos et al. 2004; Hauschild et al. 2012; Hochberg et al. 2006; Mulliken et al. 2008a, 2008b; Musallam et al. 2004; Pohlmeyer et al. 2007; Serruya et al. 2002). In all cases, however, the areas to harness and adapt the signal from must be selected a priori, often based on the known properties of the area(s) and the computational strengths of that region for motor or cognitive control (or both) that many years of research have revealed.

In the domain of noninvasive BCI methods involving humans and the event-related signals from surface electrodes [e.g., electroencephalography (EEG) or near-infrared spectroscopy (NIRS)], methods have been developed that also harness and adapt the signal from various cortical regions (Wolpaw and McFarland 1994; Wolpaw et al. 1991, 2002) to exert volitional control over an external event linked to a computer (Cherian et al. 2011; Huggins et al. 1999; Levine et al. 1999, 2000). Such tasks have involved, for example, navigating the cursor through a maze (Huang et al. 2009), controlling a wheel chair (Choi 2012; Yamada et al. 2010; Zhao et al. 2009), selecting letters on a display to produce text (Rivet et al. 2010), or performing motor imagery to guide an external direction in general (Bell et al. 2008; Contreras-Vidal et al. 2010; Kamousi et al. 2007; Onose et al. 2012; Qin et al. 2004; Shan et al. 2012), among others. As with the spike and LFP signals, the methods using the event-related potentials can provide in several contexts accurate and reliable control of the external events when the brain regions are determined a priori and the signals from such regions are harnessed and coadapted in real time with the control states of the external device.

A line of basic research that has been less explored in BCI/BMI is the possibility of using a simple directional task involving intentional control to automatically recruit a particular region of the brain and to further parcellate the recruitment into subregions within that region according to the task demands. In such a scenario, it would be useful to assess the abstract nature of the evoked signal, i.e., its robustness and/or ability to generalize the task solution across different sensory modalities, even for sensory modalities not used during the training. It would also be useful to contrast the features of the performance that depend on the type of sensory input used for guidance in closed feedback loops. We hypothesize that per-

Address for reprint requests and other correspondence: E. B. Torres, Rutgers Univ., Psychology Dept. (Busch Campus), 152 Frelinghuysen Rd., Piscataway, NJ 08854 (e-mail: ebtorres@rci.rutgers.edu).

formance accuracy achieved under external guidance from one sensory modality will transfer to another sensory modality for which the subjects were not trained.

Under a very simple binary design, based on an abstract, amodal directional signal, we ask if activation of a particular brain region or network could be automatically recruited with intentional and volitional control of our thoughts, independently of the sensory modality used for instruction and feedback. Specifically, we ask to what extent the map adapted to solve the intentional task generalizes across different forms of sensory guidance. We contrast aspects of performance that remain invariant to the type of external sensory input used for guidance and features of the performance that specifically depend on the external sensory feedback type.

We report the results of using a sparse probit classifier (Balakrishnan and Madigan 2008; Ding and Harrison 2011; Figueiredo 2003; Shevade and Keerthi 2003) to automatically uncover brain activation patterns that maximize accurate and fast performance in a simple binary directional control task. Using the visual modality for training/testing while validating as well in the auditory modality (novel to the participants), we found that although the auditory modality recruits the same area with comparable levels of strength and performance accuracy, it significantly decreases the response latency. Moreover, across modalities, during the training trials, strong coupling emerged between the prefrontal and parietal cortices in the low-frequency band for both visual and auditory modalities. Yet, at the alpha- and beta-frequency bands we found differences between the visual and the auditory modalities. The results are discussed in light of different self-emerging patterns of activation evoked in an automatic parcellation of different Brodmann's areas within the prefrontal cortex across participants. We suggest using such evoked signal as a putative marker of different types of executive control that emerge as a function of task demands.

MATERIALS AND METHODS

Participants

Nineteen participants of college educational level (ages 29.00 ± 7.01 yr, 11 men and 8 women) participated in this experiment. All of the participants in this study signed the consent form approved by the Rutgers University Institutional Review Board in compliance with the Declaration of Helsinki.

Apparatus

Subjects sat comfortably in front of a computer screen (Fig. 1*A*) wearing a head cap system to measure electroencephalographic activity (EEG). The Active Two multichannel, high-resolution biopotential measurement system built by BioSemi (Amsterdam, The Netherlands; http://www.biosemi.com/index.htm) recorded the scalp signals at a 256-Hz sampling rate from 64 channels using the

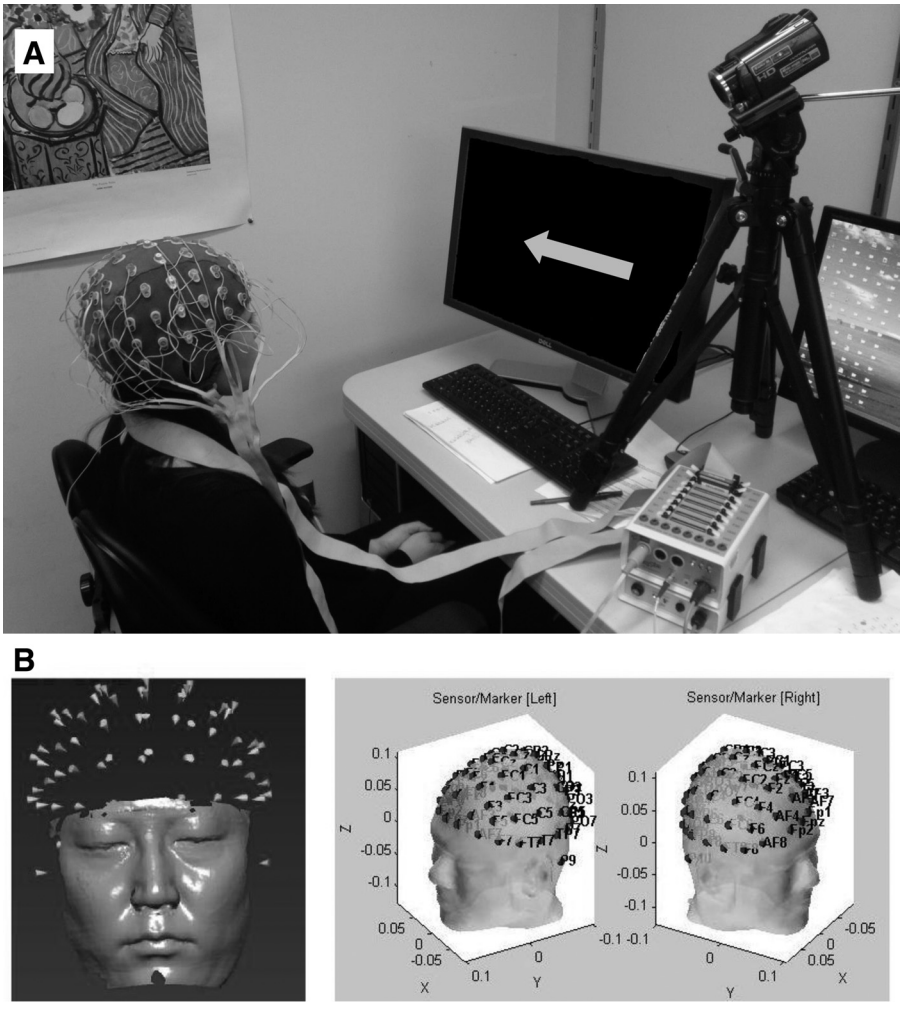

Fig. 1. Apparatus and methods. *A*: experimental setup with subject comfortably seated facing the screen monitor. Head cap has 64 channels to record EEG activity in response to the imagination of a visually instructed direction (arrow). *B*, *left*: face and head scanned using the FastSCAN scanner. Three important anatomic landmarks (nasion, gray square; left periauricular and right periauricular points, gray arrowheads) were measured with a FASTRAK stylus along with the physical positions of the 64 channels. *Right*, results of registering these data with structural MRI data using in-house developed program.

international 10-20 system. The Polhemus (Colchester, VT) hand-held FastSCAN SCORPION laser scanner system was used to track the three-dimensional physical position and orientation of the 64 channels in the subjects' head cap during calibration. The FastSCAN has a built-in FASTRAK motion capture system with 6 degrees of freedom (df), capable of recording position and orientation at 120 Hz. It also uses an ergonomic stylus for precise physical localization of each landmark (http://www.polhemus.com). Figure 1*B* shows the scanned head and face of one of the subjects with the electrodes' locations registered on the head model.

Experimental Design

The experiment consists of three phases: *1*) open-loop training (no feedback from the performance), where we estimate the currents but do not yet train the classifier algorithm; *2*) closed-loop training (real-time feedback from the performance), where both the participant and the classifier algorithm are trained; and *3*) testing based on real-time feedback (visual-trained vs. auditory-naive), where the feedback is obtained by attempting to deliberately control the cursor direction using the internally generated brain activity and the external sensory input.

The training phase is guided by visual input with an arrow shown on the screen monitor. The arrow points to one of two locations, right or left, to indicate to the subject the direction that he or she has to imagine and intend to move the cursor toward. In the open-loop version of the training phase, the subject imagines the instructed direction but receives no feedback from the outcome of this imagination exercise. Figure 2*A* shows the schematics of the epochs of the open-loop training phase. Two seconds of fixation were followed by 4 s of display of the direction that the subject had to imagine (left or right) randomly presented. The last epoch was the resting phase, lasting 4 s. The total trial lasted 10 s. The EEG activity during this open-loop training phase is used as baseline to later help adapt the signal and to correctly tune the performance outcome. There are 7 blocks of 30 trials each during this open-loop training phase.

In the visual version of the closed-loop portion of the training phase, the subjects receive instantaneous visual feedback on their performance in the form of a cursor that moves to the direction instructed by the arrow as the subject imagines the direction, or that fails to move in the imagined direction. There is no auditory feedback in this session. Since a coadaptation process is undergone between the EEG real-time signal and the subject's performance via the visual feedback of the real-time moving cursor, there is a learning progression. The subject receives feedback from this learning progression after each trial. The visual feedback of the animation of the cursor moving left or right informs the subject of success or failure accompanied by the text string "success" or "failure" (Fig. 2*B*, *right*). Seven blocks of 30 trials each are used to train the subject's EEG signal in closed-loop with the cursor feedback. At the end of each block of trials, the subject is also informed of the percent correct to help keep track of the learning rates. As with the open-loop phase, the training phase of the closed-loop phase lasts 35 min.

Validation with novel sensory modality. Five of the participants returned to perform the task using auditory input and feedback. To this end they were blindfolded and heard the instructions of the desired direction through a speaker in front of them saying "left" or "right." If the participant successfully moved the cursor in the correct direction, the speaker emitted a beep and said "good!" Otherwise, no auditory feedback was provided. All participants were naive to the auditory form of the task. The question here was to what extent the performance (accuracy and latency) and brain area recruitment from the visual domain transferred to the auditory domain.

General Explanation of the EEG-Based BMI Paradigm

Figure 3 shows the overall configuration of the real-time BMI system used in this study. In what follows we refer to the term "activity" or "activation" in relation to estimated current as it changes over time, i.e., a time series of current values. This activity is estimated first in reference to the open-loop condition, which provides the seed for estimated current values before the closed-loop training.

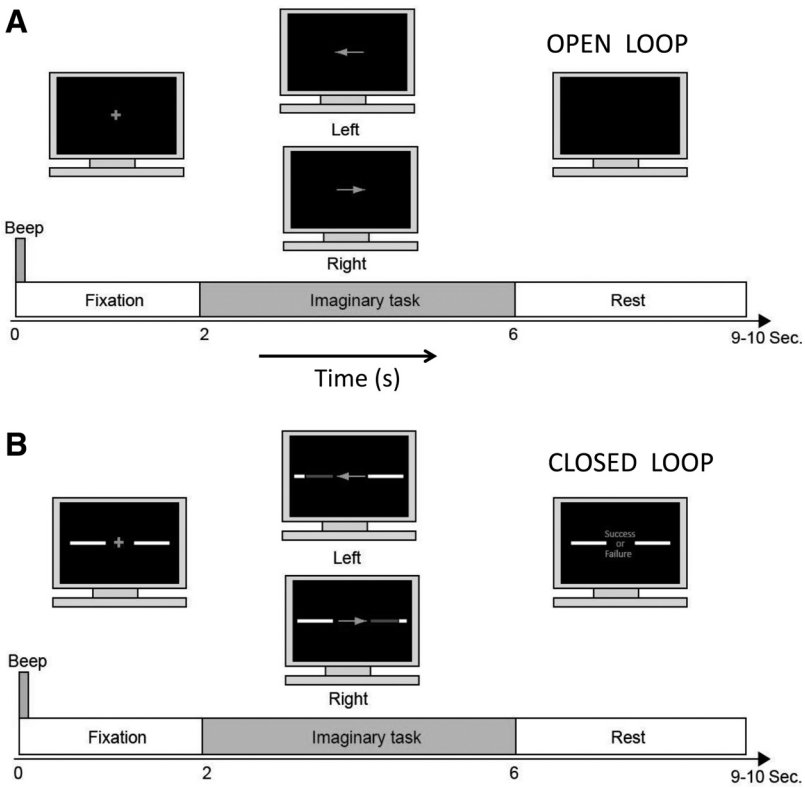

Fig. 2. Experimental design of brain executive cursor control. *A*: open-loop version of the training phase where no feedback of the performance is provided. Epochs of 1 trial include fixation on a cross (2 s), imagination task (4 s), and resting phase (4 s). *B*: closed-loop version of the training phase (brain control) provides the subject with feedback on the performance of trying to correctly move the cursor, according to the instructed direction, by thinking about that direction. The EEG signal is adapted from trial to trial according to the classifier algorithm to accurately control the motion of the cursor in real time in compliance with the instructed direction of the arrow displayed on the monitor. In the visual feedback condition (shown), the subject receives instantaneous visual feedback from the real-time performance in each trial by shifting the white cursor, aiming for the direction of the arrow. At trial completion the subject sees a "success" or "failure" message on the monitor. At the end of each of 7 blocks (after 30 trials in each block) the subject receives feedback on the success rate (%correct). In the auditory feedback condition, the subject is blindfolded and receives instructions and feedback on the performance outcome through computer speakers. Instructions are the prerecorded phrases "left" or "right" (randomly instructed from trial to trial) and "beep-good" in the case of success or "beep only" in the case of failure.

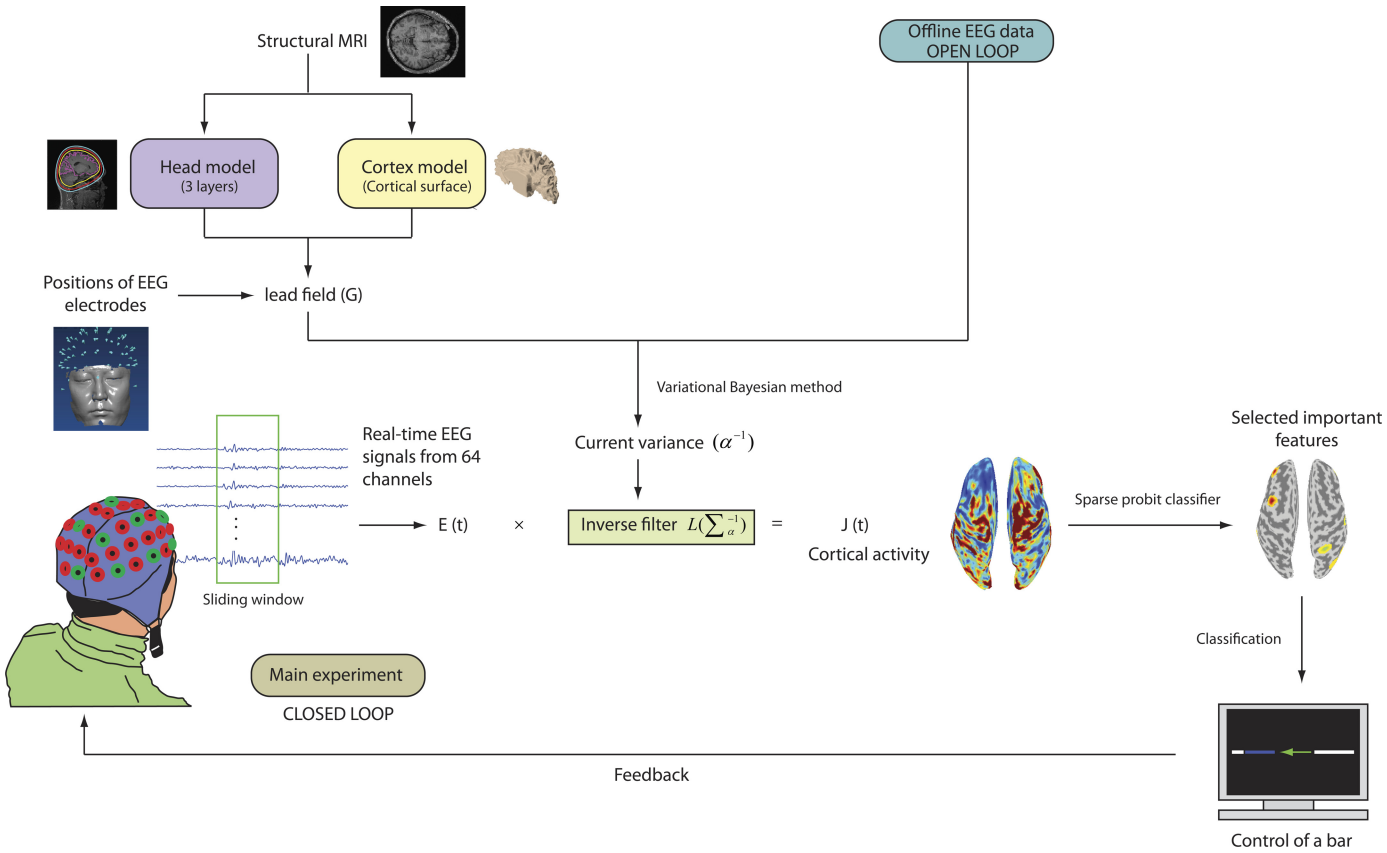

Fig. 3. General concept of brain-machine interfaces (BMI) using EEG data. The baseline EEG data analyzed offline (from the open-loop segment of the training phase) is used in combination with the head model data from the subject. To build the head model data, the structural MRI template, previously obtained, is used in combination with the head model (3 layers) and the cortex model. These data are used to fit to the actual physical positions and orientations of the electrodes obtained for each subject as shown in Fig. 1*C*. The real-time data are processed using variational Bayesian methods with a sliding window of 125 ms and passed through an inverse filter to obtain the cortical activation (estimated currents). A sparse probit classifier is used to select important features of the data (i.e., the cortical regions). These are the cortical regions where maximal activation is evoked by the closed-loop training task. The bar on the screen moves in real time as the subject thinks "left" or "right," according to the minimization of the error between the desired direction of the arrow on the monitor and the actual resulting direction from the control algorithm. Instantaneous visual feedback is provided to the subject from the real-time performance, and the %correct is displayed for each trial (see MATERIALS AND METHODS for further details). In the auditory feedback condition, no visual feedback is provided as the blindfolded subject is instructed of the desired direction and the outcome performance via speakers.

In each block we then train the classifier algorithm and track the resulting activation during the task relative to the resting state of the block. We describe the unfolding activation across each of the seven blocks of the training phases of the closed-loop conditions, where both the participant and the classifier algorithm are trained. We also examine the grand average across all experimental testing sessions and, using statistical methods, compare the strength levels across the regions that the classifier automatically recruits to test for significant differences.

There are five main steps in the estimation: *1*) registering the EEG signal with the cortical surface model using the three-layer head model (brain, skull, and scalp) to estimate the lead field matrix G to obtain the forward map from the current sources to the 64 sites of the electrodes; *2*) estimating the forward map in the open-loop version of the training phase to establish a baseline estimate of the variance of the current, which will be adapted next in the closed-loop phase of the training; *3*) estimating the inverse filter to generate the cortical activity given the EEG signal; *4*) selecting the relevant cortical features (the relevant brain regions) that lead to the successful classification of the desired direction to shift the cursor correctly; and *5*) updating the filters and classifiers continuously in real time using a sliding window of 125 ms to maximize the probability of correctly controlling the motion of the bar to the desired direction. *Steps 1* and *2* are offline in the open-loop version of the training phase to establish baseline information for each subject. *Step 3* is performed once in the offline, open-loop phase, and then *steps 3–5* are performed in the closed-loop variants of the training, to adapt the filters and classifiers appropriately. The resulting signal can be tracked on the cortical surface as the subject learns the task in real time. Also, the evolution of brain activity can be tracked after a certain number of trials or plotted as an averaged activation across all 210 trials (30 trials per 7 blocks).

Preparatory steps to create the baseline seed information for the closed-loop real-time phase. The participant's structural MRI data and EEG data during the open-loop phase are required in this step. The structural MRI gives information about the position and direction of cortical dipoles. The head model and cortical model are registered with the structural MRI. In the head model, the three layers of the brain, skull, and scalp are extracted. The boundaries between brain, skull, and scalp are generated using the Curry 6 software (Compumedics USA, Charlotte, NC). In the images in Fig. 4*A*, the yellow line represents the surface of the brain, the red line depicts the skull, and the blue line shows the surface of the scalp. Figure 4*B* shows the generated three-layer tessellated boundary surface. In the head model, the relative conductivities of the brain, skull, and scalp are 1, 0.0125, and 1, respectively.

In generating the cortex surface model, the cortical source space is extracted from the structural MRI data using the BrainVoyager software (Brain Innovation, Maastricht, The Netherlands). In this model, simultaneous activation of the pyramidal cortical neurons, located perpendicularly on the cortical surface, is believed to be the main

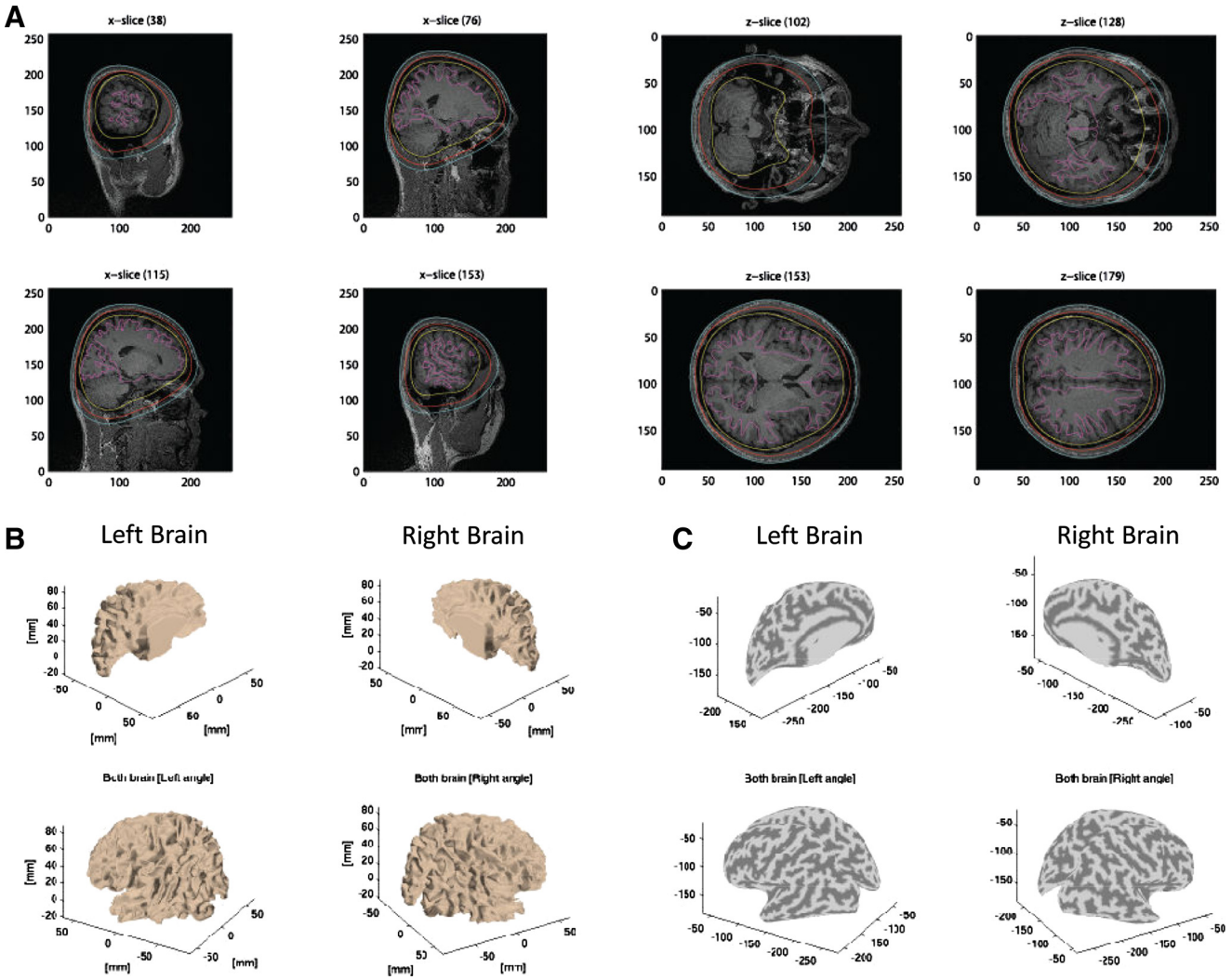

Fig. 4. Steps for registering the subject's cortical activation and brain surface. *A*: 3 layers generated using Curry 6 software (yellow line, brain; red line, skull; and blue line, scalp). *B*: original cortical surface extracted by BrainVoyager (units in mm). *C*: inflated cortical surface (units in pixels).

generator of the EEG signals. Thus many researches use this physiological assumption as a basic anatomical constraint in EEG source imaging (Babiloni et al. 2001; Dale et al. 2000; Dale and Sereno 1993; Kincses et al. 1999; Phillips et al. 1997, 2002). To impose the anatomical constraints, many dipolar sources are located over the cortical surface extracted from the structural MRI data. For computational efficiency the 400,000 original cortical vertices are downsampled to 2,240 vertices. Figure 4*B* shows the original cortical surface extracted by BrainVoyager. Figure 4*C* depicts the inflated cortical surface that will be used to register with the cortical activations extracted by the algorithms.

The first problem to solve is to estimate the lead field matrix G that relates source locations with EEG electrodes. This is related to estimating the forward map from the source locations to the signals recorded by the electrodes (64 in this case). The lead field matrix G is obtained using a realistic geometric head model (Sarvas 1987) and a first-order node-based boundary element method (BEM) (Ermer et al. 2001; Mosher et al. 1999). The EEG signal is obtained in the open-loop version of the training phase is then used to estimate the baseline variance of the current using Bayesian variational methods (Attias 1999; Sato 2010). The current's variance from the EEG activity in the open-loop phase is used to calculate an inverse filter (which will be updated later in the closed-loop phase). Figure 5*A* shows the activation registered on the cortical surface model during the open-loop phase for each instructed direction. When subjects are instructed to move the bar to the left, Brodmann's areas (BA) 6L and 6R are activated. When subjects are instructed to move the bar to the right, BA 6R is activated.

Updating steps to adapt the filter and classifier in real time during the closed-loop phase. The EEG signal from the 64 channels is used with a sliding window of 125 ms (Yamada et al. 2010; Zhao et al. 2009) across the 4 s of the closed-loop trial to update the current's variance and adapt the inverse filter used in the estimation of the cortical activation over the 2,240 vertices in real time. A sparse probit classifier (Balakrishnan and Madigan 2008; Ding and Harrison 2011) is then used to automatically extract the activation of the cortical regions that maximize the probability of correctly classifying the right or left desired direction (randomly instructed in each trial.) Maximally useful features are those that lead to the bar on the monitor being correctly shifted to the desired direction by the sparse probit classification result. Figure 5*B* shows the useful features selected by the classifier colored-coded by the weights. The visualization of the movement of the bar gives the participant real-time feedback on the correctness of the imagination task. At the end of the 30-trial block the participant gets feedback on the percent correct to keep track of the performance rate, as well.

Estimation of cortical activities from EEG signals. Equation 1 provides the computation of the estimated cortical activity J. The inverse filter L (a matrix of dimensions $2{,}240 \times 64$) uses the estimated Σ_{α}^{-1} denoting the source covariance matrix as its input, calculated as

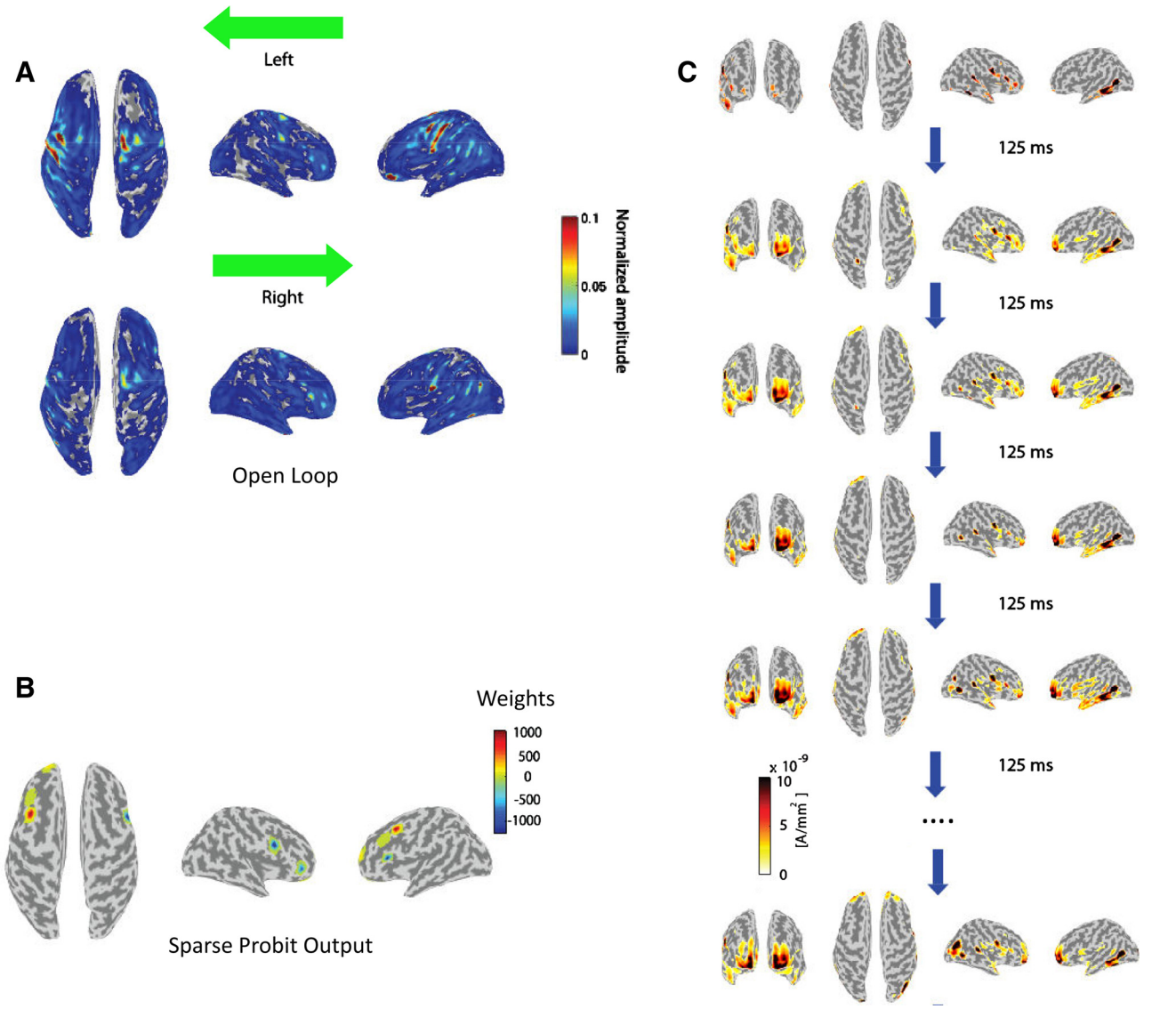

Fig. 5. Extraction of cortical signal evoked by the executive control of the cursor. *A*: cortical activity estimated from the EEG signals measured during the baseline, when the participant performs the imagination of left and right direction in the open-loop version of the training phase. *B*: extraction of the most relevant sites to correctly control the cursor in real time. These relevant features for brain control of the cursor direction concentrated in the prefrontal cortex. *C*: schematics of the algorithm for the estimation of the cortical activation $J(t)$ every 125 ms, which is input to the sparse probit classifier to adapt in real time the weights determining the features that maximize the probability of correctly classifying the intended cursor direction.

$\Sigma_\alpha^{-1} = diag(\alpha^{-1})$, where α^{-1} is 2,240 × 2,240. These α_{ij} values are unknown parameters estimated from the measured EEG data by applying a hierarchical prior (Neal 1996). The lead field matrix G is 64 × 2,240, and G' denotes the transpose. I_M represents the identity matrix of 64 × 64 (number of sensors), and β^{-1}, also 64 × 64, corresponds to the inverse of the noise variance of the observed EEG signals.

$$L\left(\Sigma_\alpha^{-1}\right) = \Sigma_\alpha^{-1} \cdot G' \cdot \left(G \cdot \Sigma_\alpha^{-1} \cdot G' + \beta^{-1} I_M\right)^{-1},$$
$$J(t) = L\left(\Sigma_\alpha^{-1}\right) \cdot E(t) \qquad (1)$$

where $E(t)$ represents measured real-time EEG signals given by 64 × 256 Hz (sampling rate), and $J(t)$ denotes the estimated cortical activities every second and is given by 2,240 × 256 Hz entries. A sliding window of 125 ms is used in real time to update these matrices during the closed-loop phase. This updating process is represented in Fig. 5*C* and illustrated with an example from the adaptation progress of a participant.

The activities in the closed loop are averaged each second (*Eq. 2*) and used as the input of a sparse probit classifier:

$$\overline{J_i} = \frac{1}{N_{\text{sample}}} \sum_{t=1}^{N_{\text{sample}}} J_i(t) \qquad (2)$$

In *Eq. 2*, N_{sample} is 256, and i indicates the ith dipole's current.

Classification of left and right directional imagery from the estimated cortical activities. The learning problem that this task has to resolve comprises two well-known issues: *1*) complexity of the learned function relating real-time EEG to the cursor control, and *2*) generalization of this function (map) estimated under the training set to new data not used in the training set (Figueiredo 2003). The function obtained during the training phase is evaluated by how well it generalizes to the novel data, often under the assumption of a common underlying probability distribution as the training data. In this work a Bayesian sparse probit classifier with the automatic relevance determination (ARD) prior was used both to avoid the

over-fitting problem related to the complexity issue and to increase generalization ability (Shevade and Keerthi 2003).

To classify the left and right directional imagery from the cortical activities estimated over 2,240 vertexes, *Eq. 3* was used:

$$x(t) = \sum_{i=1}^{N_{\text{source}}} w_i \times \overline{J}_i(t) + w_0, \quad (3)$$

where $\overline{J}_i(t)$ represents the average of the estimated cortical activities for 1 s, $x(t)$ is the result of the left or right directional imagery, and w_i denotes the weights of the classifier, decided by the sparse probit classifier (illustrated in Fig. 5*B*). N_{source} represents the number of useful cortical activities in the classification selected by the sparse probit classifier, and w_0 is an offset weight value determined for each subject. Since the sparse probit classifier automatically selects only useful cortical activities in the precise sense of correctly classifying the left or the right directional motor imagery for cursor control, the method addresses the over-fitting problem.

Figure 5*B* shows the task-relevant cortical features selected by the sparse probit classifier as the participant conducts the closed-loop version of the training phase. Here we learn that important task-relevant features are localized in areas of the prefrontal cortex. The next questions are *1*) to what extent does this task induce activation in the prefrontal cortex above and beyond the levels of activation in the rest of the brain areas, *2*) are there areas systematically selected by the classifier within the prefrontal cortex where activation is significantly higher than the overall levels in the prefrontal cortex, and *3*) how does the result from the visual cursor feedback generalize to receiving novel feedback from another sensory modality (such as auditory) under which the subject did not train?

Explicitly controlling for the inevitable eye movements in this task. Before the patterns of cortical activation selected by the sparse probit classifier and their possible generalization to other sensory modalities are examined, it is necessary to address possible motion artifacts.

The activities of the 64 channels are first sampled in the open-loop training session, with a baseline correction (−1∼0 s). The EEG signals are then bandpass filtered between 0.5 and 30 Hz using a fifth-order Butterworth filter. To remove any potential artifact caused by eye movement, a two-step method is applied. The first step is to allocate extra dipoles on the eyes, thus estimating the cortical activities on the eyes (Croft et al. 2005). In the second step, the EEG signals that correlated with eye movement are estimated from electro-occulography (EOG) signals by a linear regression and subtracted from the measured whole EEG signals to minimize the effect of eye movement (Croft et al. 2005).

In addition to controlling for general movement artifacts as explained above, we addressed which cortical areas would be explicitly recruited and driven by the task of deliberately moving the eyes in the instructed right or left directions, since these directions are randomly presented. During the imagination task, even when subjects are instructed not to move their eyes, the eyes inevitably move at times. We needed to determine the levels of EEG activation induced by the eye movements in the worst case scenario (always moving the eyes deliberately), because their motions could produce signal that would contaminate those of the regions selected by the sparse probit classifier that maximized the success probability of mentally controlling the motion direction of the cursor. In other words, we needed to verify if the eye-movement signal alone was significantly higher than the signal generated by the imagination task to drive the signal in the region of interest evoked by the cursor-control task.

Tracking Performance Accuracy, Response Latency, and Brain Activity Across Blocks

We examined the progression of learning to mentally control the cursor for each sensory modality. To this end, for each participant, the percent trials correct and the number of milliseconds that it took to respond in each of the seven blocks of the closed-loop control experiments were obtained. The learning progression was assessed through the variability of the latencies of response in each sensory modality. In tandem with the performance accuracy and response latency, we tracked the brain activation patterns across blocks in each participant and also on average across participants.

Latency of Response Variability During Feedback-Based Testing

To assess the learning progression in this task, we obtained the frequency distributions of the response latencies in each sensory modality (visual and auditory). These turned out to be non-unimodal according to the Hartigan dip test of unimodality (Hartigan and Hartigan 1985) (dip > 0.1, P approximating 0 in each subject). Two modes of the frequency histograms emerged, with latencies below 500 ms and above 500 ms. In both cases the frequency histograms were skewed. We examined each mode separately because the data split ∼50–50% of the 210 trials. In both cases there were significant differences across the seven learning blocks according to the nonparametric Kruskal-Wallis test (6 df; visual: $\chi^2 = 98.1$, $P < 6.2 \times 10^{-19}$ and auditory: $\chi^2 = 86.6$, $P < 2.4 \times 10^{-16}$ for the longer latencies; and visual: $\chi^2 = 276.8$, $P < 7.3 \times 10^{-57}$ and auditory: $\chi^2 = 170.8$, $P < 3.03 \times 10^{-34}$ for the shorter latencies).

We further examined the patterns of variability by applying distributional analyses. We used maximum likelihood estimation to estimate with 95% confidence the parameters of the probability distribution best fitting the frequency histogram of each mode. We used the continuous gamma family of probability distributions and estimated the shape (a) and the scale (b) of the distribution with 95% confidence intervals for each parameter. We also obtained estimates of the mean ($a*b$) and the variance ($a*b^2$). We obtained the Fano factor, the variance over the mean ratio to track over the seven blocks the noise-to-signal ratio as the participant improved the performance accuracy and as the stochastic signatures of the response latency variability shifted along a trajectory on the gamma plane spanned by the shape vs. scale dimensions.

Assessing Interactions Between Brain Regions and Across Hemispheres

We examined interregion relations under the different forms of sensory feedback during the closed-loop experiments. Recall that in the visual feedback version the subjects did not receive auditory input. Likewise, in the auditory feedback version they did not receive visual feedback (because they were blindfolded.) These controlled conditions were amenable to test which of the recruited areas would couple during the performance that was deprived of vision or deprived of sound. We asked if there were areas that would synchronize in both cases, despite differences in the dominant form of sensory feedback for guidance. We also asked if there were synchronization patterns unique to each form of sensory guidance. To this end we used the phase locking value (PLV) combined with the phase lag index (PLI) commonly used in signal analyses from EEG/MEG data (Aydore et al. 2013).

The PLV is the absolute value of the mean phase difference between the two signals being compared, expressed as a complex unit-length vector (Lachaux et al. 1999; Mormann et al. 2000). The PLV takes values on [0, 1] with 0 reflecting the case where there is no phase synchrony and 1 where the relative phase between the two signals is identical in all trials. PLV can therefore be viewed as a measure of trial to trial variability in the relative phases of two signals. When the signals are independent and the marginal distributions of the two signals are uniform, the relative phase will also distribute uniformly and the value of the PLV will be 0. If, on the other hand, the phases of the two signals are strongly coupled, then the PLV will approach 1. We first ensure that the marginal distributions are uniform, and then we also obtain the PLI. The PLI has been designed to

address a weakness of the PLV (Stam et al. 2007). When electrode pairs that share a common reference or that have overlapping lead field sensitivities are compared, or when cortical current density maps of limited resolution are compared, the PLV is known to suffer from linear mixing, in which the same source can contribute to both channels. The apparent phase locking in such cases may be accompanied by the relative phases concentrated around 0. The PLI is robust to the common-source problem.

The PLI quantifies the asymmetry of the relative phase distribution about 0. It takes values on the interval [0, 1]. It is 0 if the distribution of relative phase is symmetric about 0 or π. It will produce large values only when the relative phase is packed away from 0.

We used nonparametric estimates of PLV and PLI defined by others (Aydore et al. 2013; Stam et al. 2007) by averaging over trials. For the estimated PLV we used

$$\mathrm{PLV}_{\mathrm{sample}} \stackrel{\Delta}{=} \left| \frac{1}{N} \sum_{n=1}^{N} e^{i\Delta\phi_n(t)} \right|,$$

where n indexes the trial number and N is the total number of trials (210 trials in our case for each participant). We then obtain averages and standard error across all 15 participants. The corresponding nonparametric estimate of the PLI that we used was

$$\mathrm{PLI}_{\mathrm{sample}} \stackrel{\Delta}{=} \left| \frac{1}{N} \sum_{n=1}^{N} \mathrm{sign}\left[\Delta\phi_n(t)\right] \right|,$$

with n and N as defined above and the relative phase obtained as

$$\Delta\phi(t) = \arg\left[\frac{z_1(t) z_2^*(t)}{\left|z_1(t)\right| \left|z_2(t)\right|} \right],$$

where $z_1(t)$ and $z_2(t)$ are the two signals of interest when the Hilbert transform is applied to the two original signals $s_1(t)$ and $s_2(t)$ that we bandpass filtered in this case to the frequency range above 0.5 Hz and below 30 Hz.

Once the EEG data were mapped back to the cortex using the inverse mapping procedure previously described, we used the PLV and PLI to estimate interactions between time series averaged over cortical regions of interest. We chose the cortical region of interest specifically in relation to the evolution of activation strength in cortical regions over time, as the participants mastered the task. These included the prefrontal cortex, BA 17 (visual area recruited in the visual feedback version), BA 41–42 (auditory area recruited in the auditory feedback version), and BA 40 [association area of the parietal cortex, recruited in both versions of the task and known to be relevant in sensory integration, conscious motor intention, goal-directed planning, and forward prediction (Buneo and Andersen 2006; Desmurget et al. 2009; Desmurget and Sirigu 2012; Hauschild et al. 2012; Mulliken et al. 2008b)], all of which were required in this task.

In addition to the assessment of possible synchronous patterns across automatically recruited regions of interest and for different frequency bands, we also examined interhemispheric relations to unveil possible asymmetric patterns of activation between corresponding areas across brain hemispheres. To this end we statistically compared activation patterns from each cortical region automatically recruited by the algorithm on the left hemisphere to the corresponding region in the right hemisphere.

Assessing the Balance Between the Participant's and the Algorithm's Performance

We addressed whether the coadaptation process that took place was mostly driven by the performance of the person (%accuracy feedback) or by the algorithm (estimated weights). Both sets of values evolved over time, so we obtained their rates of change and determined the course of these derivatives using a simple ratio, $r = \Delta A/\Delta W$. In the case of the weight vector, we normalized it to obtain a unit vector and computed the norm of the change from one block to another. Likewise, with the percent accuracy, we obtained the block-by-block changes and set the values in the [0, 1] range. If $r > 1$, the accuracy leads, thus suggesting that the person dominates. On the other hand, if $r < 1$, the change in weights wins. This would suggest that the algorithm dominates. We tracked this ratio across all blocks.

Exogenous vs. Endogenous Guidance in this task

Two forms of sensory guidance can be defined relative to the subject's decision in this task. One is exogenous in nature, guiding the decisions of the person primarily by external input (e.g., visual or auditory sensory feedback). The other is endogenous in nature, guiding the person's decisions primarily by the internal motions and emotions, including deliberate and spontaneous thoughts affecting the decisions as well. Both of these forms of intentionality are important because weighing them determines the outcome of the decision, thus affecting the overall performance. Given that exogenous and endogenous intentionality have different motor signatures (Torres 2011, 2013; Torres and Zipser 2002, 2004), depend on specific external or internal sources of sensory guidance (Torres et al. 2010, 2011), and possibly have different brain signatures (Andersen and Buneo 2002; Haggard 2008; Torres et al. 2013; Waszak et al. 2005), we asked to what extent we could separate, in the neural signals, aspects of the decision that were externally driven from aspects of the decision that also depended on internal intentions. To this end we examined the trials that resulted in success separately from those which resulted in failure. The success trials were compliant with the external form of sensory guidance (whether visual or auditory). In this regard, a good balance between the exogenous input and the endogenous intentions led to a successful outcome. In the error trials, however, this balance was upset somehow and the mentally driven decision failed. It may have been that the external sensory input was not correctly processed. It may have been that even though the external sensory guidance was successfully processed, some spurious spontaneous thoughts interfered with the final outcome, or that the subject's internal calculations failed or took too long, among other possible factors. In any of those hypothetical cases, it may be safe to assume that the balance between the exogenous and the endogenous sources of guidance was different than in the success cases. Thus we examined the neural activity separately and asked if such differences were also reflected in the neural code.

RESULTS

Accuracy of Performance During Feedback-Based Learning

Visually guided training and testing. All participants built up toward accurate performance with 73.33% correct at the lowest rate and 100% correct at the highest rate. Of the 19 participants, 15 had similar patterns of activation and 4 (discussed elsewhere as case studies) exhibited some differences in the levels of activation of subregions within the prefrontal cortex.

The block-by-block average performance of the 15 participants was tracked across blocks. On average, the 15 participants had increasing levels of accuracy across the 7 blocks of practice when the instructions were provided visually and the visual feedback of the cursor motion as controlled by the brain activity was provided in real time. Mean percent correct ($\pm$SD) across the 30 trials and for each of the 7 blocks was 89.28 (9.16), 90.95 (9.09), 92.37 (9.09), 95.7 (5.76), 93.56 (8.52), 95.23 (8.24), and 96.90 (4.79), with a grand average of 93.42 (6.78).

Auditory testing, blindfolded, without training. The performance of the cursor control was also tested with the use of a blindfold under auditory instructions and auditory feedback in

five randomly chosen subjects from the group of participants. There was no training for any of the cases in the auditory modality and no visual feedback. This test served as validation to address generalization of the function approximated by the algorithm relating accurate real-time performance and brain activation. The results on the accuracy were high in all subjects, despite the novelty of the stimulus and feedback type. The evolution of the accuracy as mean percent correct (±SD) across all subjects for the 7 blocks of 30 trials each was 98.0 (4.47), 99.33 (1.48), 97.33 (4.34), 97.33 (5.96), 98.66 (2.96), 98.66 (2.98), and 98.66 (1.82), with a grand total average of 98.28 (3.30). Surprisingly, all tested participants were more accurate in the auditory domain than in the visual domain, despite no training. The performance accuracy was also less variable with auditory guidance than with visual guidance (despite a smaller set of 5 participants in the auditory case).

Latency of Response During Feedback-Based Testing

Figure 6*A* shows the box plots resulting from the Kruskal-Wallis comparison of the absolute distance from each latency value to the estimated mean latency across all seven blocks. The plot in Fig. 6*A* depicts the results from analyzing the mode of the bimodal distribution of all latencies with the longest latencies (*top*, visual; *bottom*, auditory). The distributional analyses using the gamma distribution estimated parameters and tracking their shift on the gamma plane are shown in Fig. 6*B* (*top*, visual; *bottom*, auditory). The arrows represent the flow of the shifts, and the numbers are the block numbers. *Insets* in Fig. 6*B* depict the evolution of the Fano factor. The largest drops in noise occurred in the visual feedback case transitioning from *block 1* to *block 2* and then again from *block 5* to *block 6*. *Block 7* remained stable. In the case of auditory feedback, the largest drop in noise was during transitioning from *block 3* to *block 4* and then again from *block 6* to *block 7*. Similar trends with different patterns were quantified for the mode of the bimodal frequency histogram comprised by the shorter latencies (below 500 ms), which accounted for the other half of the data. Notice that these large changes in stochastic signatures would have been missed had we assumed homogeneity of variance and normal distributions of

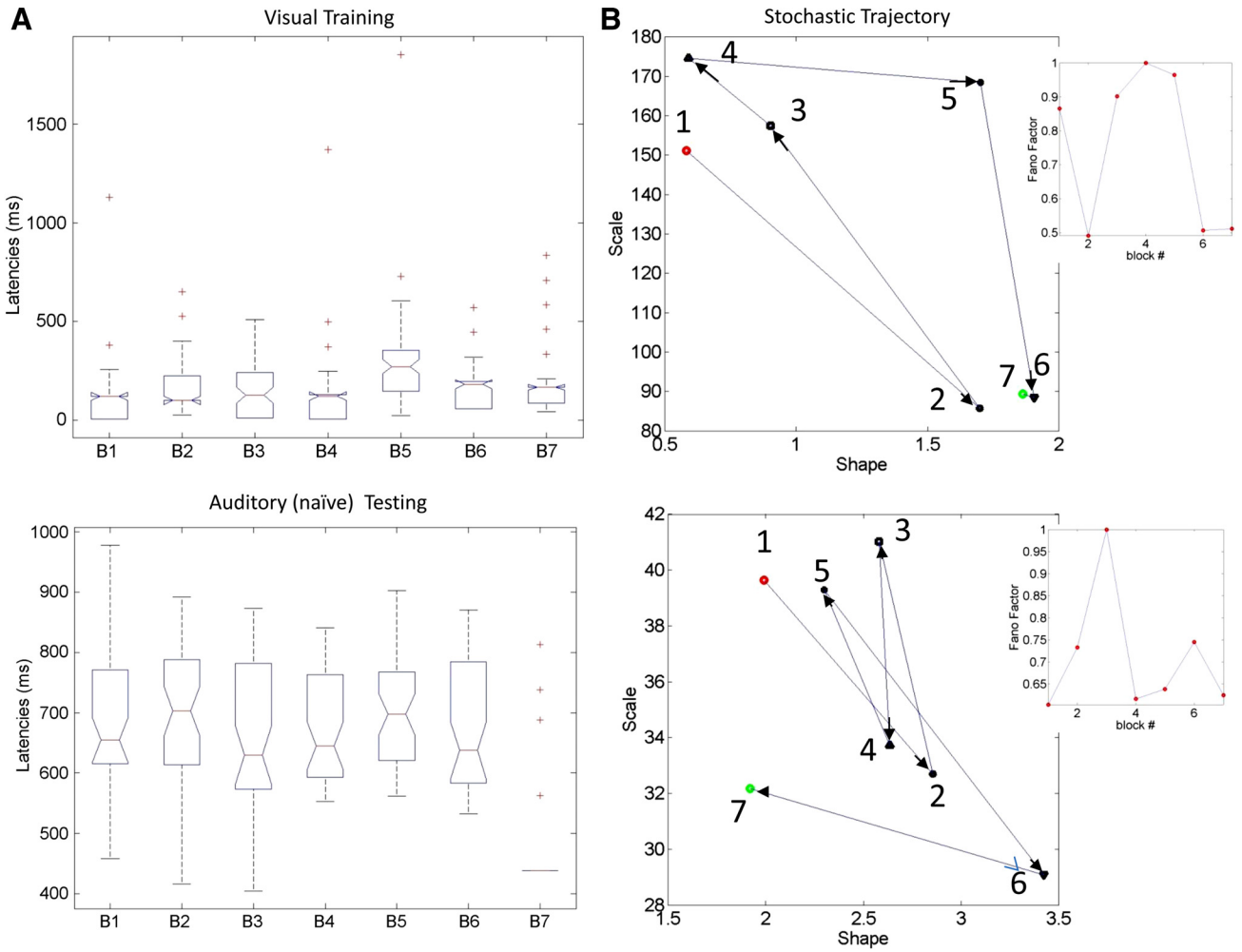

Fig. 6. Learning progression of the response latencies of the decision across 7 blocks of the closed-loop experiments, where the participants receive real-time sensory feedback to guide their performance. *A*: box plots from the Kruskal-Wallis analyses of the variability of the absolute distance from each trial latency response to the mean in each block (differences were significant, see text). Data are from the mode of larger latencies in the overall frequency distribution, which turned out to be bimodal. *Top* plot is from the visual feedback case (15 subjects), and *bottom* plot is from the auditory case (5 subjects.) *B*: stochastic trajectories showing the shifts on the gamma (shape-scale) plane in the estimated shape and scale of the frequency histogram of response latencies in each block (comprising at least 100 trials each). *Insets* show the evolution of the noise-to-signal ratio, given by the Fano factor, across all 7 blocks. *Top* plot refers to the case of visual feedback, and *bottom* plot refers to the auditory feedback.

the latencies and summarized the statistics by the mean and variance of the theoretical Gaussian distribution.

Visual Guidance on Average Recruits the Prefrontal Cortex

The averaged activation during testing across all trials and blocks showed automatic recruitment of the prefrontal cortex for each participant. Figure 7 shows 10 representative cases (for simplicity, 10 of the 15) with the typical patterns of activation for the front, top, and side views of the left and right hemispheres of the brain under visual guidance. Each participant had significantly higher activation of the prefrontal cortex than the rest of the brain [2-tailed $t(26) = 3.82$, $P < 0.01$]. Moreover, in each of the 15 participants, within the prefrontal cortex, activation of BA 9, 10, and 11 was significantly higher than that of the rest of the brain [$t(26) = 3.43$, $P < 0.01$].

Table 1 lists all subjects' mean activation values with the standard deviations for the prefrontal cortex, BA 9, 10, and 11 within the prefrontal cortex, and the corresponding activation of the rest of the brain as evoked by the intentional task that was visually guided.

Figure 8 shows the patterns of brain activation averaged across all 15 subjects for each of the sensory modalities used for guidance/feedback and for the control experiment for eye movements. The control eye-movement case (Fig. 8*A*) did not result in higher activation evoked in the prefrontal cortex. Figure 8*B* shows the averaged activation across all subjects with the typical patterns when the instructions and feedback were visual. Standard error and significance are indicated.

Auditory-Based Cursor Control Also Recruits the Prefrontal Cortex

Figure 8*C* shows the averaged activation patterns across all blocks and participants during auditory testing. Notice that despite no training in the auditory domain, the recruitment of the prefrontal cortex is comparable to that of the visually trained case, with significantly higher engagement than the rest of the brain. Although also recruited with auditory guidance, BA 9, 10, and 11 are not as highly engaged as when the visual instructions and visual feedback are used. Table 2 shows the mean activations with the standard deviations for the auditory modality. This validation test also addresses the generalization of the function (map) that

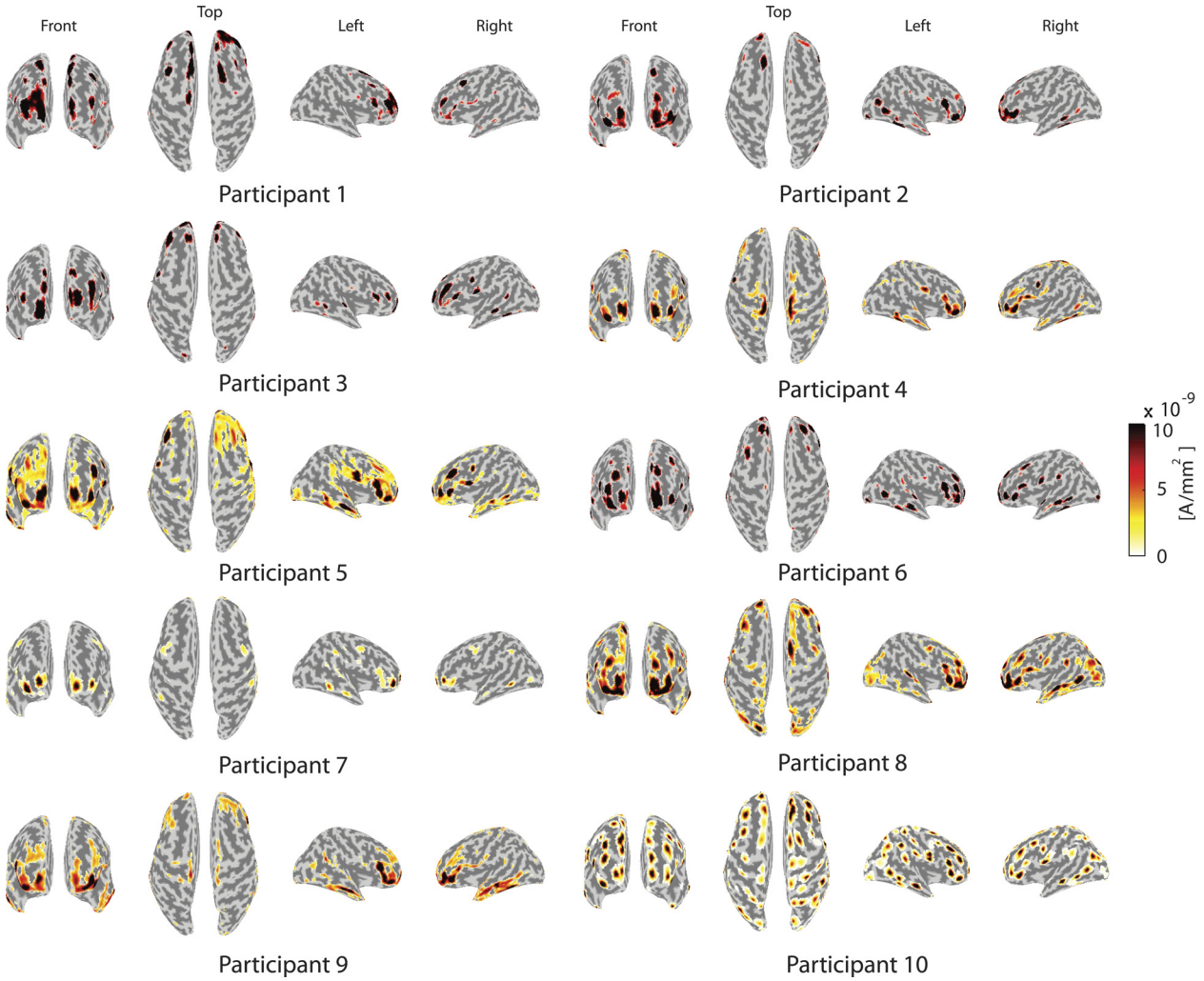

Fig. 7. Evolution of the neural activation is shown across the 7 blocks of experiment in the closed-loop condition. *Left*, the results under visual feedback without audio. *Right*, the results under auditory feedback without vision. Notice the differences between the two conditions and the recruitment of the prefrontal cortex common to both cases.

Table 1. *Cortical activation in the visually guided task*

Subject	BA 9–11	Prefrontal Cortex	Other Areas	BA 9	BA 10	BA 11
1	8.9880 (±42.823)	7.2624 (±38.207)	1.7577 (±0.96538)	7.8844 (±30.123)	12.131 (±44.188)	7.9581 (±47.431)
2	4.7579 (±14.538)	4.9846 (±23.320)	2.3088 (±12.271)	2.4851 (±0.98775)	7.2790 (±27.748)	4.6557 (±5.4612)
3	19.710 (±87.291)	9.8079 (±52.650)	2.7309 (±12.892)	7.8009 (±20.645)	34.005 (±91.220)	18.620 (±104.09)
4	3.1181 (±9.6147	3.1288 (±10.165)	1.7901 (±2.4931)	1.5376 (±0.31998)	4.1515 (±14.151)	3.4147 (±9.1441)
5	4.1428 (±11.534)	4.7064 (±18.048)	1.6858 (±2.7826)	2.3280 (±0.88121)	5.5414 (±16.226)	4.3753 (±11.520)
6	8.1417 (±40.035)	5.6984 (±27.713)	2.0211 (±7.166)	5.6857 (±16.448)	11.486 (±44.906)	7.7147 (±45.578)
7	9.3849 (±47.441)	7.3106 (±42.437)	2.7977 (±6.2171)	2.6952 (±1.1049)	18.867 (±83.971)	8.0309 (±30.011)
8	5.7925 (±22.026)	4.2599 (±14.886)	2.1303 (±6.4351)	2.4023 (±1.4198)	5.7778 (±24.024)	7.5688 (±26.097)
9	2.7636 (±2.3585)	2.9993 (±7.0069)	1.8876 (±1.7119)	2.2314 (±0.6645)	2.7246 (±2.9982)	3.0612 (±2.4994)
10	14.293 (±62.957)	14.036 (±67.186)	5.4079 (±33.919)	27.380 (±87.829)	20.384 (±75.840)	4.3540 (±29.772)
11	5.1682 (±21.405)	5.9484 (±27.540)	2.5406 (±11.637)	3.4682 (±1.8665)	9.5268 (±1.8665)	3.8284 (±4.1786)
12	6.4129 (±4.3419)	5.1781 (±3.4957)	2.5439 (±1.4056)	4.1425 (±1.2458)	5.3047 (±2.6665)	8.1636 (±5.2436)
13	23.240 (±93.158)	24.053 (±215.15)	3.8476 (±12.164)	11.094 (±12.483)	52.568 (±175.57)	14.594 (±34.936)
14	18.537 (±88.138)	15.466 (±21.010)	4.2049 (±7.3619)	15.402 (±20.157)	16.729 (±11.686)	14.854 (±24.785)
15	34.608 (±180.56)	55.167 (±416.72)	4.1051 (±30.077)	14.427 (±46.760)	99.700 (±348.19)	11.883 (±17.234)

Values are mean activation (± SD) in nA/mm^2.

the algorithm developed in real time between the brain activation and the cursor performance.

Unfolding the Activation Across Blocks as the System Learns

The overall patterns of brain activation in the testing were revealing of the prefrontal cortex as a critical node in accurate control of the instructed cursor direction across sensory modalities. But what was the course of activation leading to that result? As it turned out, the evolution of the automatic recruitment of brain areas was different across experimental blocks of the training session. They also differed between visual and auditory guidance during the training.

Figure 9 tracks the evolution of the brain activation in each block, averaged across all 15 subjects. Notice that both forms of sensory guidance in this task, on average, across blocks, recruited the prefrontal cortex at higher levels than the rest of the brain. However, across the learning progression this task also engaged other sensory areas and shifted their activation patterns in different ways, depending on the type of sensory feedback used for guidance. Other regions recruited across the blocks included parts of the visual cortex (BA 17), parts of the auditory cortex (BA 41–42), and parts of the parietal cortex (BA 40). We then asked if there was any coupling between these areas as the system learned. Specifically, given the accuracy of the performance under both forms of sensory guidance, the strong differences in latency and the block-to-block variability (with the auditory case being less variable and significantly faster), we wanted to know *1*) if there was a synchronization pattern common to both the visual and auditory feedback and *2*) if there were features unique to each form of sensory guidance. We reasoned that the former might partly explain the robustness of the performance accuracy across sensory modalities, whereas the latter might be informative of differences in sensory processing that resulted in significant response latency values and variability patterns between modalities.

Coupling of Prefrontal-Parietal Areas vs. Prefrontal Visual and Prefrontal Auditory Areas Across Different Frequency Bands

We examined interrelations across four regions of interest recruited by the task during the course of adaptation and learning of the mental control of the cursor under different forms of sensory guidance. These included prefrontal cortex, visual cortex (BA 17), auditory cortex (BA 41–42), and parts of the parietal cortex (BA 40).

Figure 10 shows the PLV and PLI for both types of sensory guidance. The PLV and PLI analyses yielded strong coupling between the prefrontal region and the parietal area BA 40 for the low-frequency band (<8 Hz). Some further refinement in interregion coupling could be observed across different frequency bands. For frequencies above 0.5 Hz and below 30 Hz, there was also coupling in both conditions between the prefrontal cortex and BA 17 (visual cortex) during visual guidance and between the prefrontal cortex and BA 41–42 (auditory cortex). Likewise, according to the PLV, in the alpha band (8–12 Hz) there was coupling between parietal and visual areas under visual guidance and between parietal and auditory areas under auditory guidance. Across all frequency bands under analyses, the PLI values were well above 0, indicating diminished bias from spurious correlations from common sources. In the beta band (13–30 Hz) the patterns differed between sources of sensory guidance: prefrontal cortex showed coupling with visual and parietal areas during visual feedback, yet auditory feedback showed coupling between parietal and auditory areas.

We also used *t*-tests to compare the levels of activation between hemispheres in the parcellation of the prefrontal cortex with the highest levels of activation: BA 9R and BA 9L, BA 10R and BA 10L, and BA 11R and BA 11 L, in each subject (210 trials per experiment) for the visual feedback condition and in each of the 5 subjects for the auditory feedback case. All comparisons without exception yielded $P > 0.05$ with no significant differences that would signal strong asymmetries between hemispheres.

Algorithm vs. Subject Performance: Who Dominates?

We also tracked across blocks the relationships between the subjects' performance (changes in %accuracy) and the algorithm output (changes in weights) to determine which of the two components drove the learning and could potentially better explain the overall outcome of the experiments.

The ratio $r = \Delta A/\Delta W$ unfolded across each of the seven blocks informed of the evolution of the rate of change in performance by the subjects in relation to the weights adjusted

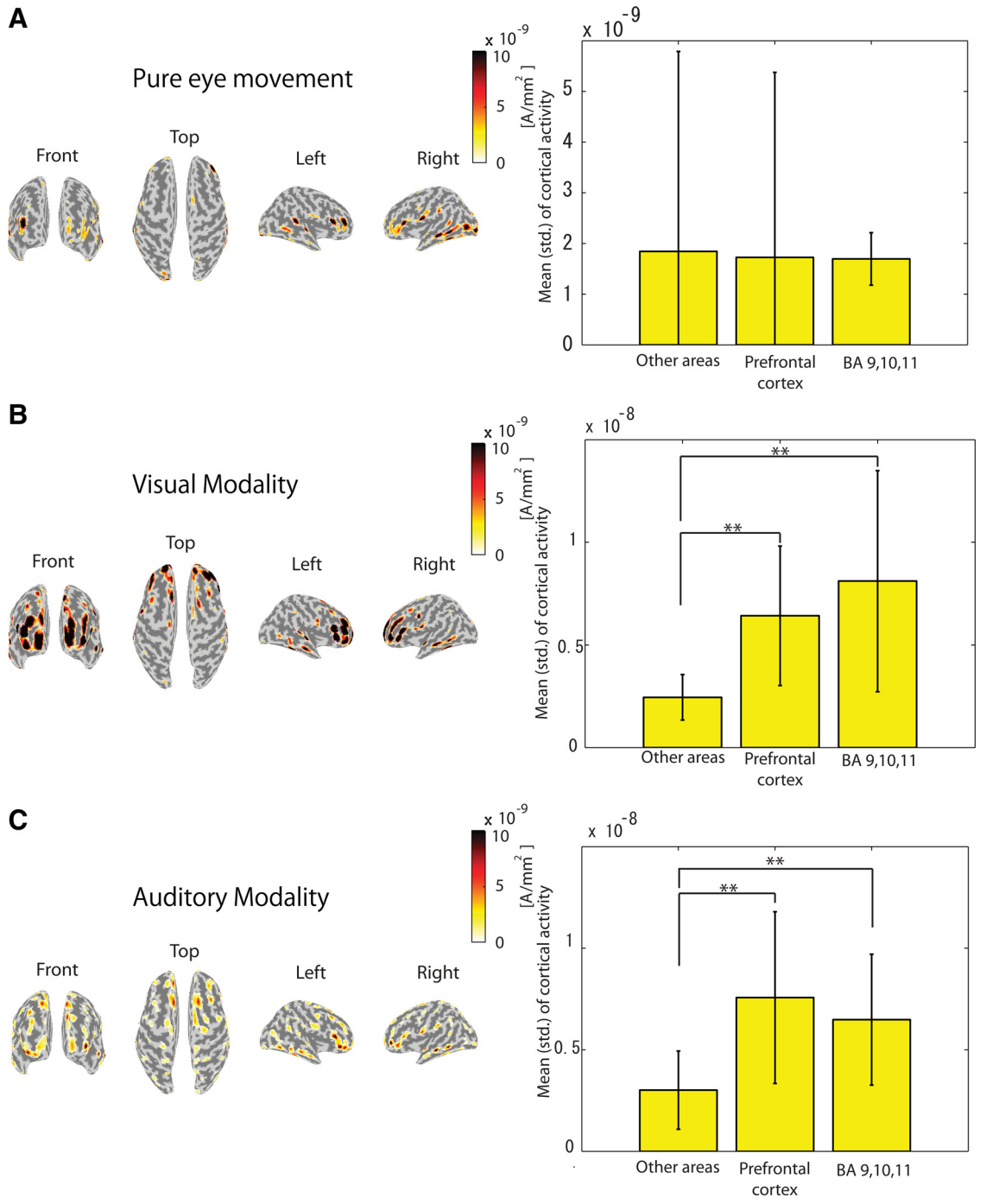

Fig. 8. Averaged activation across subjects. *A*: control test for pure eye movements reveals no significant differences in recruitment of prefrontal cortex areas in relation to the rest of the brain. *B*: on average across subjects, the visually driven control task recruits the prefrontal cortex and particularly Brodmann's areas (BA) 9, 10, and 11 with patterns of activation significantly above the rest of the brain. *C*: on average, the auditory driven control task for the 5 naive subjects also recruited the prefrontal cortex above the rest of the brain. Activation of BA 9, 10, and 11 was also higher than that of the rest of the brain but not higher than that of the rest of the prefrontal cortex, as in the visually driven case.

by the algorithm. A ratio >1 indicates that the subject's performance dominated, whereas a ratio <1 indicates that the algorithm dominated the outcome. Figure 11*A* shows the outcome of this metric for visual (*left*) and auditory feedback (*right*). The ratio in the visual case is taken over all 15 subjects, whereas in the auditory case it is taken over 5 subjects (ergo the higher variability). In the visual case the averaged ratio remained below 1 (except when *block 7* is compared with *block 6*). This suggests that the algorithm drove the learning through *blocks 1–6*. In contrast, the auditory feedback showed an averaged ratio above 1 in the first 3 comparisons involving *blocks 1–4* and below 1 in the fourth and fifth comparisons involving *blocks 3*, *4*, and *5*. The last comparison, between *blocks 6* and *7*, went above 1 again, thus suggesting that the subjects dominated the overall outcome in the auditory testing. It is remarkable that in both cases

Table 2. *Cortical activation in the auditory version of the task measured in 5 of the 15 typical participants*

Subject	BA 9–11	Prefrontal Cortex	Other Areas	B9	B10	B11
1	11.220 (±70.286)	11.745 (±66.840)	4.5238 (±29.176)	32.409 (±131.90)	10.843 (±34.621)	0.3572 (±0.27107)
2	5.1890 (±14.569)	5.4433 (±15.798)	2.3073 (±6.4001)	2.8956 (±1.4307)	9.8659 (±27.694	3.9963 (±4.8190)
3	7.6591 (±42.276)	12.374 (±72.657)	7.6381 (±54.618)	2.4941 (±14.262)	7.9340 (±40.090)	10.213 (±51.819)
4	5.4177 (±42.684)	4.7837 (±35.801)	1.2023 (±3.3151)	3.0638 (±14.221)	1.9170 (±2.9698)	8.4343 (±59.791)
5	2.1366 (±4.8713)	2.2374 (±5.3507)	2.0132 (±4.4164)	1.6872 (±0.44475)	3.5006 (±9.5462)	1.6742 (±0.55276)

Values are mean activation (± SD) in nA/mm^2.

the accuracy of the performance was comparable, yet the response latencies differed so much. The differences in the unfolding of this ratio may, at least in part, explain such differences.

Exogenous vs. Endogenous Guidance in This Task

Figure 11, *B* and *C*, shows the results of the comparison between neural activities in successful vs. unsuccessful trials across five subjects that performed the visual (*B*) and auditory (*C*) versions of the task. The patterns of activation across the brain were very different between the successful and the error trials. Furthermore, the analyses revealed that in the case of successful performance, BA 11 (orbitofrontal cortex) was highly activated, above all other areas of the parcellation recruited in the prefrontal cortex and above the rest of the brain. This region of cortex is well known for its role in the reward system. In the error trials, BA 11 was not recruited with the same strength as in the successful cases. There, the most active area was BA10 (frontopolar cortex), known to be involved in strategic planning and cognitive branching (Christoff et al. 2001, 2003). The latter is a term describing the ability to maintain a previously running task in a pending state for subsequent retrieval and execution upon completion of the ongoing one. In this sense it may be the case that error trials driven by endogenous intentions and/or spontaneous thoughts took longer and may have contributed to longer decision latencies overall. Indeed, upon comparison we found that the latencies of the error trials were significantly longer than those of the successful trials.

Under visual feedback, the latency of response in successful trials ranged from 372.65 (±65.21) to 630.24 (±169.73) with a median of the mean values of 468.99. Yet, when only the failure trials are considered, the latency nearly tripled, with ranges from 1,115.32 (±162.08) to 1,336.23 (±250.82) with a median of the mean values of 1,175.02. Two-tailed *t*-test for visual successful trials vs. visual failure trials yielded $t(26) = -25.21$, $P < 0.01$.

Under auditory feedback, the latency in successful trials ranged from 352.22 (±18.24) to 422.54 (±41.23) with a median of the mean values of 383.58. However, when only failure trials are taken into account, the latency nearly doubled, with ranges from 739.82 (±83.24) to 808.14 (±121.96) with a

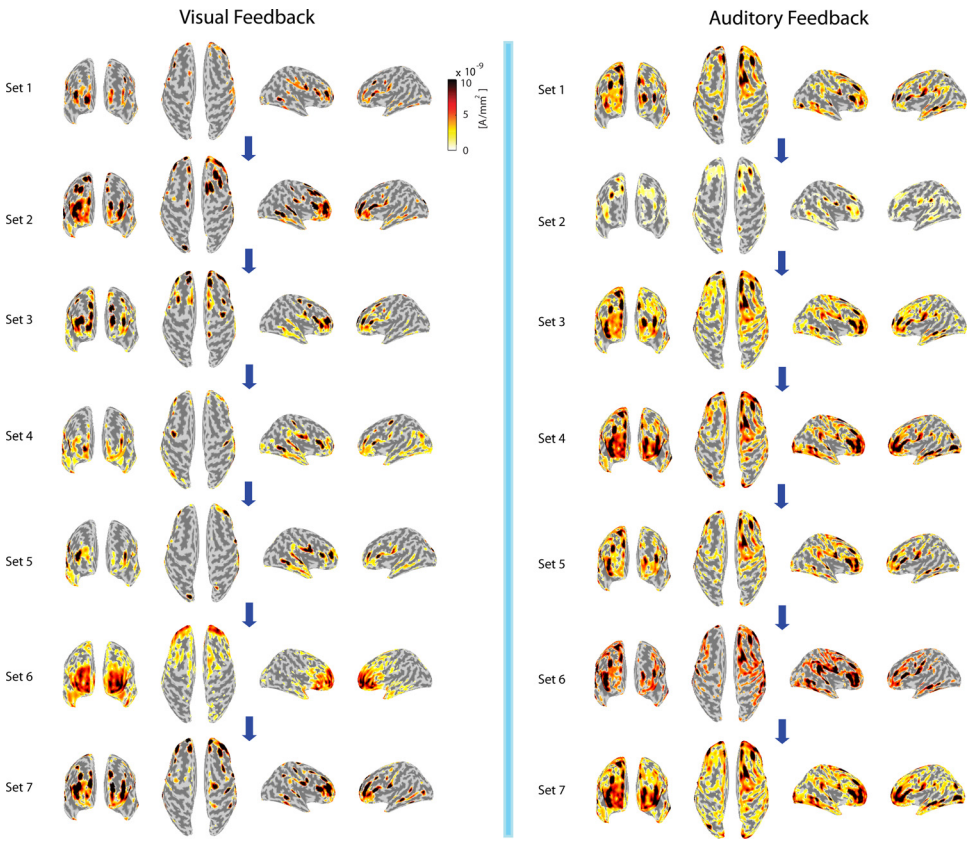

Fig. 9. Patterns of cortical activation in 10 participants (visual feedback case). Frontal, top, and side views of the 2 brain hemispheres registered with the activation according to the output of the sparse probit classifier determining the most useful features (i.e., the brain regions) that maximized the probability of successfully moving the cursor in the intended direction. The activations of the corresponding areas are highlighted (A/mm^2) as obtained on average across the 4 s of the testing block.

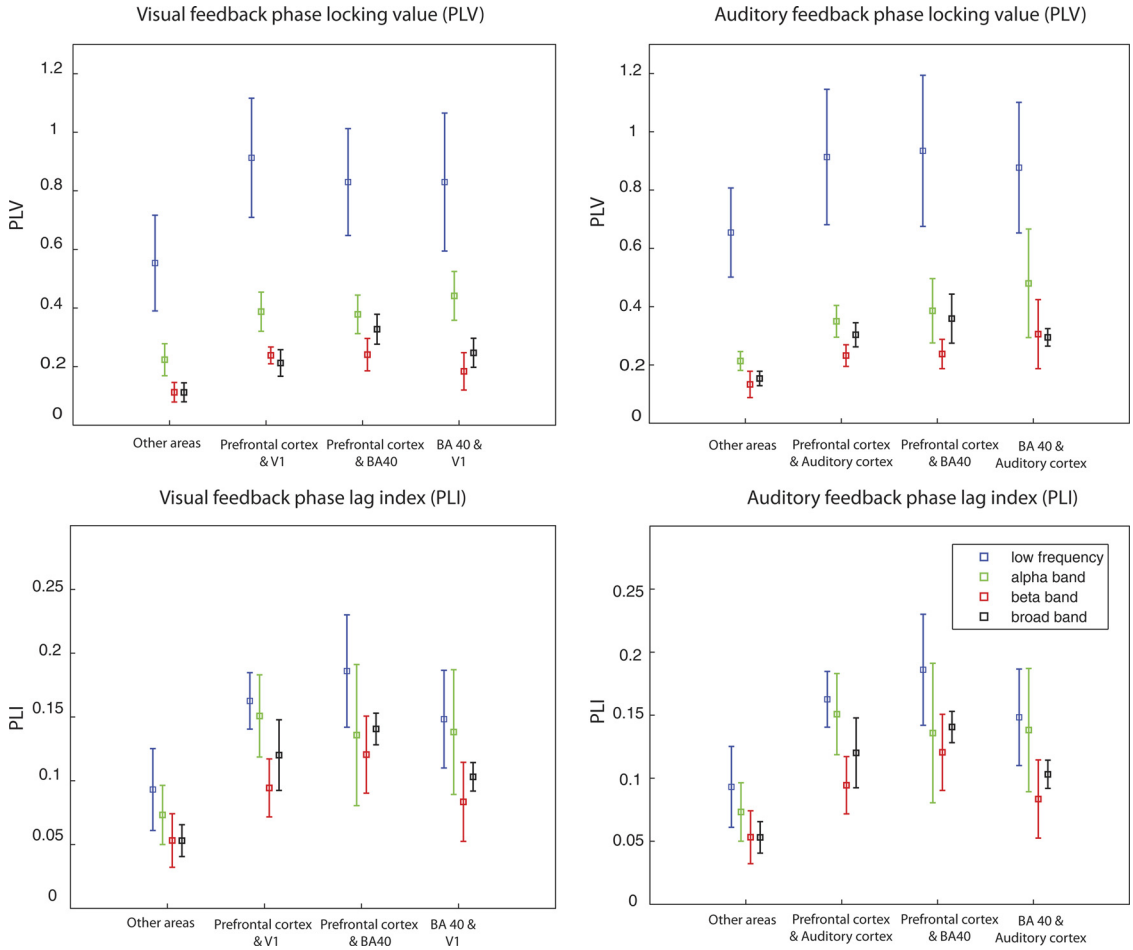

Fig. 10. Phase locking value (PLV) and phase lag index (PLI) of the main cortical regions of interest (ROI) activated during the training in relation to the rest of the brain. The ROI included the prefrontal cortex, the parietal area (BA 40), the visual areas (BA 17), and the auditory areas (BA 41–42). The frequency bands used in the analyses are indicated. Low-frequency band (<8 Hz) showed the strongest coupling between the frontoparietal nodes, followed by coupling in the alpha band (8–13 Hz) between BA 40 and visual cortex in the visual feedback case and by BA 40 and auditory cortex in the auditory feedback case. In the beta band (13–30 Hz), B40-visual cortex in the visual feedback case and B40-auditory cortex in the auditory feedback case were most coupled. In the broad frequency band (0.5–30 Hz), both conditions showed coupling in the frontoparietal nodes, with differences across conditions between visual and prefrontal cortex (in the visual feedback case) and auditory and prefrontal cortex (in the auditory feedback case).

median of the mean values of 769.18. Two-tailed t-test for auditory successful trials vs. auditory failure trials yielded $t(6) = -18.48$, $P < 0.01$.

Comparison across modalities also yielded statistically significant differences with two-tailed t-test for visual successful trials vs. auditory successful trials yielding $t(16) = 2.2161$, $P < 0.05$, and two-tailed t-test for visual failure trials vs. auditory failure trials yielding $t(16) = 10.5319$, $P < 0.01$.

DISCUSSION

We explored in this work the possibility of automatically recruiting cortical regions important for the intentional control of direction. We set out to ask if we could find strong activation patterns in some brain region that would be conducive of accurate performance while also well generalizing the solution map to novel forms of external sensory guidance. We specifically hypothesized that accuracy achieved under external guidance from one sensory modality would transfer to another sensory modality, one for which the subjects were not trained.

We found support for the automatic recruitment of a cortical region during this task that, during the testing phase of the BCI experiment, remained robust to changes in the external source of sensory guidance and for which the accuracy of the subjects' performance was maintained. We further found that upon learning, the response latencies depended on the type of sensory guidance used as real-time feedback. Specifically, in the absence of sounds the visually guided task had longer response latencies than the auditory version of the task, which the subjects performed in the absence of vision. The high accuracy in the visually guided task seemed driven by the classifier (according to the unfolding of changes in accuracy and changes in weights). However, during the sound-guided test the subjects dominated over the classifier. We report on the evolution of the course of adaptation of the subject's performance and of the classifier's weight adaptation. We also report on the overall grand-averaged test performance of this task.

To uncover the map relating the electrophysiological signal and the real-time cursor control, we used a Bayesian sparse probit classifier with the automatic relevance determination (ARD) prior (Balakrishnan and Madigan 2008; Ding and Harrison 2011). To the best of our knowledge, this family of classifiers had not been used in the context of BCI. However,

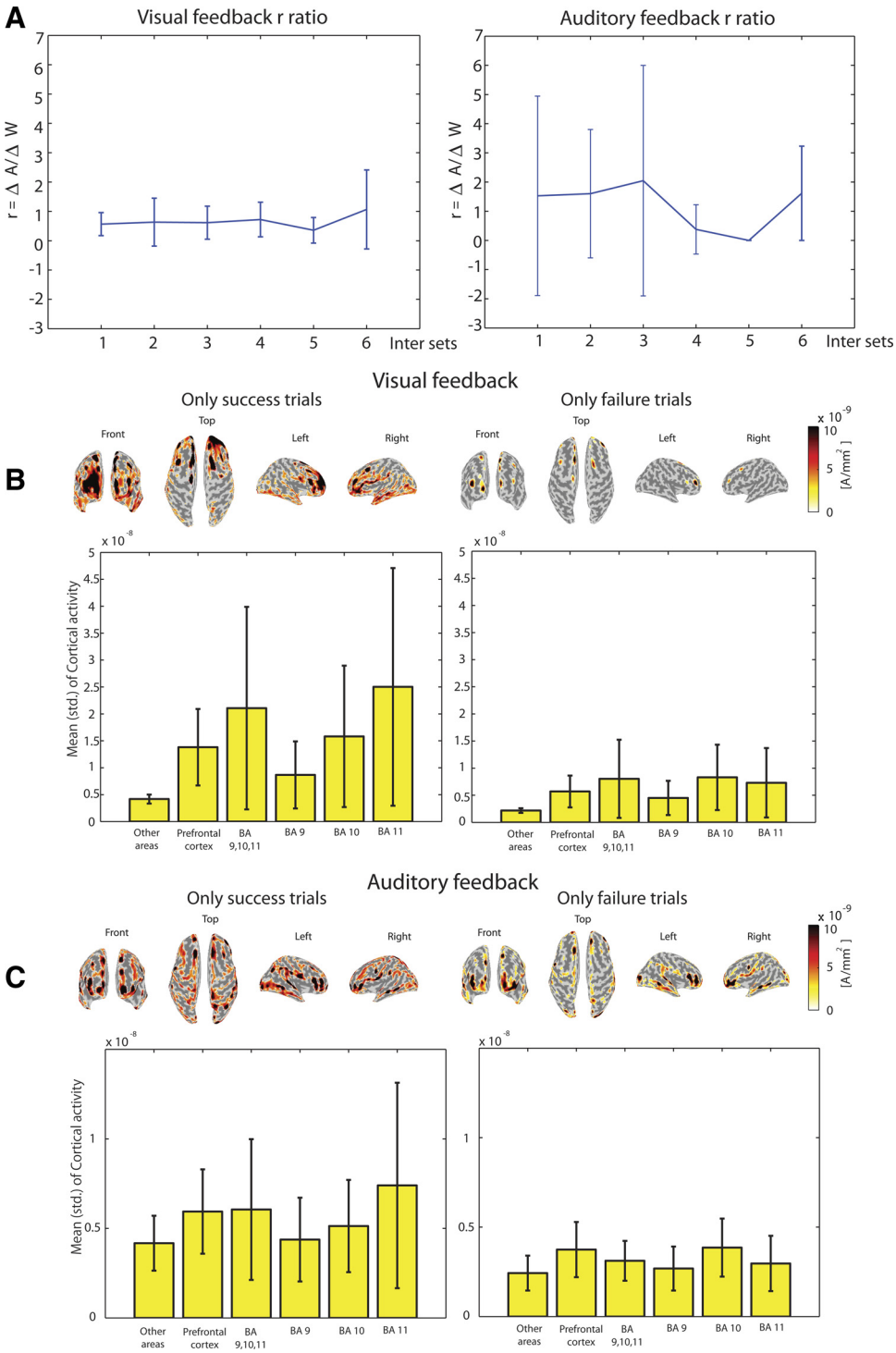

Fig. 11. Other features of the performance. *A*: the ratio $r = \Delta A/\Delta W$ across blocks of training to determine if the subject or the algorithm drives the performance. *Left* plot shows the visual feedback case where the ratio remains below 1 in all but the last comparison. This indicates that the algorithm drives the performance. *Right* plot shows the auditory feedback case where the ratio is above 1 in most blocks, suggesting that the subjects drive the performance. *B*: comparison of activation levels in the prefrontal cortex, the parcellation of BA 9, 10, and 11, and other brain areas when successful and unsuccessful trials are grouped. Notice the differences in strength levels and activation patterns throughout the brain. Success trials recruit orbitofrontal cortex (OFC; B11), whereas error trials do not. Error trials recruit B10 with higher activity.

we were motivated to employ this technique on the EEG signal to address the complexity issues related to the real-time coadaptation of the map between the external signal and the brain activation. We also know that in other learning settings, this type of classifier avoids the over-fitting problem and increases generalization abilities (Figueiredo 2003; Shevade and Keerthi 2003). Thus, in the context of EEG, we wanted to know if specific cortical regions would be automatically recruited by this binary directional control task. We also wanted to know if such automatic recruitment would generalize to a new sensory modality, one for which the subjects had not trained.

The Bayesian sparse probit classifier selects the cortical activation features that maximize the probability of correctly controlling the direction of the computer cursor at will. Across all participants we found that the classifier systematically and automatically identified the maximally useful features (the brain regions) in the prefrontal cortex with significantly stronger levels of activation in that area than in the rest of the brain.

Upon training under visual guidance, the signal maximizing accurate task performance was automatically identified in the prefrontal cortex within the context of visual instructions and visual feedback. Similar recruitment of the prefrontal cortex was also quantified during the auditory feedback test, with a conservation of accuracy level despite no training with sounds. Furthermore, under both visual and auditory guidance, we found a parcellation of areas within the prefrontal cortex recruited with higher levels of strength than the rest of the brain. These comprised the dorsolateral prefrontal cortex (DLPF), the frontopolar (rostrolateral) cortex, and the orbitofrontal cortex (OFC), corresponding to Brodmann's areas 9, 10, and 11, respectively.

Under visual guidance, these regions of the prefrontal cortex were automatically recruited with higher activation than the rest of the prefrontal cortex in all 15 participants. We had 4 outliers who also recruited the prefrontal cortex with higher activation than the rest of the brain, but who had a different parcellation of activation strength in BA 9, 10, and 11 with respect to the rest of the group. We reserve the analyses and further study of that subgroup for another report. In what follows, we refer only to the 15 participants that revealed similar parcellation and strength levels of the prefrontal cortex.

The recruitment by this simple task of the prefrontal cortex above and beyond the levels of activation of the rest of the brain was evident in all participants. This was the case for both the visual and the auditory versions of the task (performed in 1/3 of the participants), despite the lack of training in the auditory case. Given that this task required volitional control of thoughts, executive control, multitasking, the buffering of prior information, and the comparison between internally generated information and externally available information to improve future performance (among other cognitive demands), the robustness of the accuracy suggests that an aspect of the performance was invariant to the sensory input type. Arguably, this would render that component of the signal "amodal" in the precise sense that its directional accuracy remained invariant. In this sense, this task may have uncovered an abstract signal representing key aspects of exogenously driven intentional control.

In contrast to the overall accuracy invariably quantified across different types of sensory feedback, the latency of the response strongly depended on the sensory modality used in real-time guidance. Auditory feedback was conducive of much faster responses with far less variability than the responses guided by visual feedback. We were very careful to test this hypothesis in a controlled manner, whereby only one form of input was present. Under such conditions, for each one of the subjects we found strong differences in latency. It was interesting that during performance guided by auditory feedback, the subjects dominated over the classifier, as quantified by the accuracy change-to-weight change ratio tracking the rates of change of these parameters across the experimental blocks.

It could be argued that the neural correlate of directional "intentionality" that we propose to have uncovered in the prefrontal cortex is primarily driven by exogenous sensory input. Would the activation patterns be different in trials where internally generated (endogenous) input drove the response? To address this question, we analyzed separately the successful and the unsuccessful trials. In the former, the exogenous input successfully guided the decision and the internal computations were timely and contributed to the maximization of success and the changes in the classifier that ultimately singled out the prefrontal region as a key player for the success of this task. In the latter, however, internal sensory guidance, including the spontaneous thoughts and mental computations leading to error, won over the external guidance, or the external sensory guidance was not properly integrated in a timely fashion along with the internal processes needed to solve the task, among other possible factors. Regardless of the combination of factors leading to failure, the cortical regions recruited during failure and their activation strengths were significantly different from those recruited during the successful trials. Furthermore, the latencies of response errors more than doubled in both sensory modalities. This result strongly suggests that no automatic decisions were taking place and that no fast random choices were being made either. Instead, a deliberate, slow process seemed to have taken place in the failure trials that utilized all sources of guidance (endogenous and exogenous) but failed to timely achieve the correct goal.

To further explore what types of processes may have taken place during the learning progression ultimately leading to an overall success in the task and to a good generalization, we examined the patterns of performance (accuracy and latency) and the corresponding brain activation patterns as the blocks unfolded. The evolution of the activation across the blocks revealed a recruitment of the areas of the parietal region BA 40 along with parts of visual and auditory regions, BA 17 and BA 41–42, respectively. Further analyses of PLV and PLI revealed strong coupling of the frontoparietal network at low-frequency band (<8 Hz), and this was also found with more modest values for the broad frequency band (<0.5 Hz and >30 Hz). This network had been reported before in nonhuman primates (Buschman and Miller 2007), where an interchange between deliberate top-down and automatic bottom-up processes unfolded during attentional control. Attentional control was indeed required to master this task under both visual and auditory guidance. Previous work in nonhuman primates situates areas of the parietal cortex as necessary for forward estimation in directionally driven control (Andersen and Cui 2009; Mulliken et al. 2008b). In humans, this region has been linked to intentional control (Naghavi and Nyberg 2005; Newman et al. 2003), also required by this task.

In humans, it has been argued that conscious intention and motor awareness arise in the parietal areas prior to impending acts (Desmurget et al. 2009; Desmurget and Sirigu 2009). Although our task did not require overtly moving, motor imagery may have taken place before the signal turned abstract (abstract in the precise sense that it correctly generalized to the external auditory modality for which the subjects had not been trained). All subjects unanimously reported that initially they explicitly thought of the instructed direction, yet as their accuracy reached reliable indexes, they found themselves not even thinking about it. Some very fast automatic decision took place that led to a correct outcome. This is also suggested by the short latencies of the correct trials, particularly in the auditory case. Differences between visual and auditory performance were also found in the alpha frequency band, where parietal and visual regions or parietal and auditory regions were modestly coupled during the visually and auditory-guided versions of the task, respectively.

In addition the unfolding progression of the activation in key regions to solve this task and the coupling of the frontoparietal network, we discuss the parcellation of the prefrontal cortex that the learning revealed overall, when averaged across all blocks of the testing blocks. The highest activation levels of the prefrontal regions were found in the DLPF, the frontopolar cortex, and the OFC, corresponding to BA 9, 10, and 11, respectively.

The higher-strength levels found in the DLPFC, the frontopolar cortex, and the portion of the OFC across all participants invites various lines of further investigation. A connection between the DLPF cortex and the reward system via the OFC axis has been suggested, in addition to connections to other brain areas including the thalamus and the dorsal caudate nucleus of the basal ganglia (Groenewegen et al. 1990), the hippocampal formation and the parahippocampal cortex (Goldman-Rakic et al. 1984), and the primary and secondary association areas of the neocortex (including the posterior temporal, parietal, and occipital areas; Petrides and Pandya 1999). Two of the nodes of this network, the DLPF cortex and the OFC, were recruited by this task in the averaged activation patterns, and as the activity unfolded over time, areas of the parietal-frontal node were also recruited in tandem. These nodes appear to be critical for executive control and to be active once the system has mastered the task. Of particular interest in this regard was the higher activation of OFC quantified in the correct trials. It appears that correctly performing the task and receiving feedback from the performance selectively engaged BA 11. Such a result could have consequences for cognitive remediation therapies.

In the early stages of the learning this task could have evoked motor imagery. One of the regions of the prefrontal cortex that was automatically recruited here, the DLPF cortex, is also reported as an important area for motor planning, organization, and regulation of actions, particularly during tasks that require executive control. Although this task did not require overt movements, its directionality control may have evoked motor imagery in its early learning stages (as subjectively reported by the subjects), before the signal emerged as an abstract, general solution map from the visual to the novel auditory modality. Indeed, the auditory modality also engaged this region significantly more than the rest of the brain. The DLPF area has been said to be critical for aspects of social interactions (Amann et al. 2012; Baddeley and Wilson 1988; Kamei et al. 2008, 2010; Perfetti et al. 2010), including the decoding of intentionality, executive memory, and general abstract thinking required to navigate complex social dynamics in real time.

The frontopolar prefrontal cortex (BA 10), also called rostrolateral or anterior region, was recruited by this task across all subjects. This area is reported to be the largest cytoarchitectonic area in the human brain and is poorly understood in terms of function (Ramnani and Owen 2004). It is thought to be implicated in strategic processes in memory recall and executive function, particularly in relation to top-down control (Burgess et al. 2007a, 2007b; Weidner et al. 2009) and the ability to maintain a previously running task in a pending state for subsequent retrieval and execution on completion of the ongoing one. Interestingly, the error trials recruited this region and accounted as well for the increase in the variability of the latency across trials. The response latencies were found to be significantly longer in the error trials, possibly suggesting lengthier computations that failed to be completed on time.

It has been proposed that the DLPF and the frontopolar cortices interact and form a hierarchical system specialized for the evaluation, monitoring, and manipulation of information held in working memory (Christoff et al. 2001, 2003). Specifically, it has been suggested that the frontopolar cortex is recruited in addition to the DLPF cortex when internally generated information being acted on is not present in the external environment. This sort of buffering of internally generated information is required in the present task, because participants in real time had to try to improve current performance based on prior successes. Likewise, executive function to decide on the proper directional thought was required by the task. Indeed, decision making has been associated with the frontopolar region (Koechlin and Hyafil 2007), specifically during reasoning tasks (Norman and Shallice 1986) and inductive inferences requiring evaluation of self-generated information during judgment of frequencies and recency (Milner et al. 1991). These aspects of cognitive control were necessary as well to master the present task.

The frontopolar cortex is also critical in humans for multitasking and planning ahead (Dreher et al. 2008) as well as for episodic future thinking (Irish et al. 2013). In nonhuman primates, this area of the prefrontal cortex has been said to play a major role in high-level integration of information coming from visual, auditory, and somatic sensory systems to achieve amodal, abstract, conceptual interpretation of the environment (Petrides and Pandya 2006, 2007). It has been suggested that this area may be the anatomic basis for influencing abstract information processing and that it may play a role in cognitive operations requiring a balance between deliberate and spontaneous thoughts (Petrides and Pandya 2006, 2007; Sarnrhein et al. 1998; Tomberg and Desmedt 1998). In the present study the transfer of accurate performance from visual to auditory sensory modalities, even in the absence of training with auditory instructions and feedback, suggests that this region in the humans may be critical for abstract-amodal cognitive computations, as well. Interestingly, the lengthy internal computations that ultimately failed and resulted in error trials recruited this region of prefrontal cortex, as well.

Another area recruited by the task was the OFC (BA 11). In nonhuman primates this portion of the prefrontal cortex has been linked to cognitive aspects of decision making present in this task (Wallis and Miller 2003). The OFC is also thought to represent emotional states (Bechara et al. 2000; Rolls and Grabenhorst 2008) and reward (Roesch et al. 2006; Schoenbaum et al. 2006, 2011) during decision making. In this study those aspects of the task self-emerged as the participant improved performance and mastered the mind control of the cursor. In the present task the OFC was highly active above and beyond other subregions of the prefrontal cortex in the successful trials during both visual and auditory guidance.

It will be interesting to use this task with additional directions on the screen and investigate visuomotor, audiomotor and tactile motor tasks that probe different spatial directions under various degrees of perturbation. In the visuomotor domain this has been done in primary motor cortex (Chase et al. 2012; Jarosiewicz et al. 2008). Such studies have permitted the assessment of functional reorganization within a given region. We could attempt to reproduce such useful paradigms. In our

case, however, we would let the algorithms and subjects' performance exchange automatically recruit areas of cortex useful to deal with systematic perturbations of the sensory input. At the same time we could track in real time the evolution of the cortical signals during validation of naive performance. This could be achieved by using different sensory modalities, as we did in this study with the auditory and the visual feedback signals. The invariance of accuracy that we found across visual and auditory feedback paired with the strong dependencies of the response latency on the type of sensory modality for guidance places us in an advantageous position to determine individually for each performer which sensory modality that person's system naturally prefers to better guide the external cursor in the most accurate and the fastest way.

All in all, the present task, paradigm, and classification algorithms have been very revealing of possible functionality of the prefrontal cortex and the potential roles of its self-emergent parcellation in cognitive, amodal intentional control, as well as in unintended performance that also depends on other internal factors. Our results are consistent with the anatomic substrates and lesion studies reported in the literature, yet they also provide the means to explore real-time recruitment and activation levels across different nodes of the frontoparietal network, as well as to track their rates of change within these regions.

GRANTS

This work was supported by National Science Foundation Cyber-Enabled Discovery and Innovation Type I Award 0941587.

DISCLOSURES

We used code from RIKEN Brain Science Institute-Toyota Collaboration Center (BTCC) that is part of a patent application to which K. Choi contributed 25% as an inventor (Yamada H, Nakatani T, Ebe K, Cichocki A, Choi K, inventors; Toyota, applicant. *Mobile body control device and mobile control method*. Japan Patent WO 2010/050113 A1, 2010). Authorization was obtained from the Japan Patent Office to use this code for research purposes.

AUTHOR CONTRIBUTIONS

K.C. and E.B.T. conception and design of research; K.C. performed experiments; K.C. and E.B.T. analyzed data; K.C. and E.B.T. interpreted results of experiments; K.C. and E.B.T. prepared figures; K.C. and E.B.T. drafted manuscript; K.C. and E.B.T. edited and revised manuscript; K.C. and E.B.T. approved final version of manuscript.

REFERENCES

Amann B, Gomar JJ, Ortiz-Gil J, McKenna P, Sans-Sansa B, Sarro S, Moro N, Madre M, Landin-Romero R, Vieta E, Goikolea JM, Salvador R, Pomarol-Clotet E. Executive dysfunction and memory impairment in schizoaffective disorder: a comparison with bipolar disorder, schizophrenia and healthy controls. *Psychol Med* 42: 2127–2135, 2012.

Andersen RA, Buneo CA. Intentional maps in posterior parietal cortex. *Annu Rev Neurosci* 25: 189–220, 2002.

Andersen RA, Cui H. Intention, action planning, and decision making in parietal-frontal circuits. *Neuron* 63: 568–583, 2009.

Andersen RA, Burdick JW, Musallam S, Pesaran B, Cham JG. Cognitive neural prosthetics. *Trends Cogn Sci* 8: 486–493, 2004.

Attias H. Inferring parameters and structure of latent variable models by variational bayes. In: *UAI' 99 Proceedings of the Fifteenth Conference on Uncertainty in Artificial Intelligence*. San Francisco, CA: Morgan Kaufmann, 1999, p. 21–30.

Aydore S, Pantazis D, Leahy RM. A note on the phase locking value and its properties. *Neuroimage* 74: 231–244, 2013.

Babiloni F, Carducci F, Cincotti F, Del Gratta C, Pizzella V, Romani GL, Rossini PM, Tecchio F, Babiloni C. Linear inverse source estimate of combined EEG and MEG data related to voluntary movements. *Hum Brain Mapp* 14: 197–209, 2001.

Baddeley A, Wilson B. Frontal amnesia and the dysexecutive syndrome. *Brain Cogn* 7: 212–230, 1988.

Balakrishnan S, Madigan D. Algorithms for sparse linear classifiers in the massive data setting. *J Mach Learn Res* 9: 313–337, 2008.

Bechara A, Damasio H, Damasio AR. Emotion, decision making and the orbitofrontal cortex. *Cereb Cortex* 10: 295–307, 2000.

Bell CJ, Shenoy P, Chalodhorn R, Rao RP. Control of a humanoid robot by a noninvasive brain-computer interface in humans. *J Neural Eng* 5: 214–220, 2008.

Buneo CA, Andersen RA. The posterior parietal cortex: sensorimotor interface for the planning and online control of visually guided movements. *Neuropsychologia* 44: 2594–2606, 2006.

Burgess PW, Dumontheil I, Gilbert SJ. The gateway hypothesis of rostral prefrontal cortex (area 10) function. *Trends Cogn Sci* 11: 290–298, 2007a.

Burgess PW, Gilbert SJ, Dumontheil I. Function and localization within rostral prefrontal cortex (area 10). *Philos Trans R Soc Lond B Biol Sci* 362: 887–899, 2007b.

Buschman TJ, Miller EK. Top-down versus bottom-up control of attention in the prefrontal and posterior parietal cortices. *Science* 315: 1860–1862, 2007.

Carmena JM, Lebedev MA, Crist RE, O'Doherty JE, Santucci DM, Dimitrov DF, Patil PG, Henriquez CS, Nicolelis MA. Learning to control a brain-machine interface for reaching and grasping by primates. *PLoS Biol* 1: e42, 2003.

Chase SM, Kass RE, Schwartz AB. Behavioral and neural correlates of visuomotor adaptation observed through a brain-computer interface in primary motor cortex. *J Neurophysiol* 108: 624–644, 2012.

Cherian A, Krucoff MO, Miller LE. Motor cortical prediction of EMG: evidence that a kinetic brain-machine interface may be robust across altered movement dynamics. *J Neurophysiol* 106: 564–575, 2011.

Choi K. Control of a vehicle with EEG signals in real-time and system evaluation. *Eur J Appl Physiol* 112: 755–766, 2012.

Christoff K, Prabhakaran V, Dorfman J, Zhao Z, Kroger JK, Holyoak KJ, Gabrieli JD. Rostrolateral prefrontal cortex involvement in relational integration during reasoning. *Neuroimage* 14: 1136–1149, 2001.

Christoff K, Ream JM, Geddes LP, Gabrieli JD. Evaluating self-generated information: anterior prefrontal contributions to human cognition. *Behav Neurosci* 117: 1161–1168, 2003.

Contreras-Vidal JL, Bradberry TJ. Design principles for noninvasive brain-machine interfaces. *Conf Proc IEEE Eng Med Biol Soc* 2011: 4223–4226, 2011.

Contreras-Vidal JL, Bradberry TJ, Agashe H. Movement decoding from noninvasive neural signals. *Conf Proc IEEE Eng Med Biol Soc* 2010: 2825–2828, 2010.

Croft RJ, Chandler J, Barry R, Cooper NR, Clarke AR. EOG correction: a comparison of four methods. *Psychophysiology* 42: 16–24, 2005.

Dale AM, Sereno MI. Improved localization of cortical activity by combining EEG and MEG with MRI cortical surface reconstruction: a linear approach. *J Cogn Neurosci* 5: 162–176, 1993.

Dale AM, Liu AK, Fischl BR, Buckner RL, Belliveau JW, Lewine JD, Halgren E. Dynamic statistical parametric mapping: combining fMRI and MEG for high-resolution imaging of cortical activity. *Neuron* 26: 55–67, 2000.

Desmurget M, Sirigu A. A parietal-premotor network for movement intention and motor awareness. *Trends Cogn Sci* 13: 411–419, 2009.

Desmurget M, Sirigu A. Conscious motor intention emerges in the inferior parietal lobule. *Curr Opin Neurobiol* 22: 1004–1011, 2012.

Desmurget M, Reilly KT, Richard N, Szathmari A, Mottolese C, Sirigu A. Movement intention after parietal cortex stimulation in humans. *Science* 324: 811–813, 2009.

Ding Y, Harrison RF. A sparse multinomial probit model for classification. *Pattern Anal Appl* 146: 47–55, 2011.

Dreher JC, Koechlin E, Tierney M, Grafman J. Damage to the fronto-polar cortex is associated with impaired multitasking. *PLoS One* 3: e3227, 2008.

Ermer JJ, Mosher JC, Baillet S, Leah RM. Rapidly recomputable EEG forward models for realistic head shapes. *Phys Med Biol* 46: 1265–1281, 2001.

Figueiredo CP. Adaptive sparseness for supervised learning. *IEEE Trans Pattern Anal Mach Intell* 25: 1150–1159, 2003.

Goldman-Rakic PS, Selemon LD, Schwartz ML. Dual pathways connecting the dorsolateral prefrontal cortex with the hippocampal formation and

parahippocampal cortex in the rhesus monkey. *Neuroscience* 12: 719–743, 1984.

Groenewegen HJ, Berendse HW, Wolters JG, Lohman AH. The anatomical relationship of the prefrontal cortex with the striatopallidal system, the thalamus and the amygdala: evidence for a parallel organization. *Prog Brain Res* 85: 95–116; discussion 116–118, 1990.

Haggard P. Human volition: towards a neuroscience of will. *Nat Rev Neurosci* 9: 934–946, 2008.

Hartigan JA, Hartigan PM. The dip test of unimodality. *Ann Stat* 13: 70–84, 1985.

Hatsopoulos N, Joshi J, O'Leary JG. Decoding continuous and discrete motor behaviors using motor and premotor cortical ensembles. *J Neurophysiol* 92: 1165–1174, 2004.

Hauschild M, Mulliken GH, Fineman I, Loeb GE, Andersen RA. Cognitive signals for brain-machine interfaces in posterior parietal cortex include continuous 3D trajectory commands. *Proc Natl Acad Sci USA* 109: 17075–17080, 2012.

Hochberg LR, Serruya MD, Friehs GM, Mukand JA, Saleh M, Caplan AH, Branner A, Chen D, Penn RD, Donoghue JP. Neuronal ensemble control of prosthetic devices by a human with tetraplegia. *Nature* 442: 164–171, 2006.

Huang D, Lin P, Fei DY, Chen X, Bai O. EEG-based online two-dimensional cursor control. *Conf Proc IEEE Eng Med Biol Soc* 2009: 4547–4550, 2009.

Huggins JE, Levine SP, BeMent SL, Kushwaha RK, Schuh LA, Passaro EA, Rohde MM, Ross DA, Elisevich KV, Smith BJ. Detection of event-related potentials for development of a direct brain interface. *J Clin Neurophysiol* 16: 448–455, 1999.

Irish M, Hodges JR, Piguet O. Episodic future thinking is impaired in the behavioural variant of frontotemporal dementia. *Cortex* 49: 2377–2388, 2013.

Jarosiewicz B, Chase SM, Fraser GW, Velliste M, Kass RE, Schwartz AB. Functional network reorganization during learning in a brain-computer interface paradigm. *Proc Natl Acad Sci USA* 105: 19486–19491, 2008.

Kamei S, Hara M, Serizawa K, Murakami M, Mizutani T, Ishiburo M, Kawahara R, Takagi Y, Ogawa K, Yoshihashi H, Shinbo S, Suzuki Y, Yamaguchi M, Morita A, Takeshita J, Hirayanagi K. Executive dysfunction using behavioral assessment of the dysexecutive syndrome in Parkinson's disease. *Mov Disord* 23: 566–573, 2008.

Kamei S, Morita A, Serizawa K, Mizutani T, Hirayanagi K. Quantitative EEG analysis of executive dysfunction in Parkinson disease. *J Clin Neurophysiol* 27: 193–197, 2010.

Kamousi B, Amini AN, He B. Classification of motor imagery by means of cortical current density estimation and Von Neumann entropy. *J Neural Eng* 4: 17–25, 2007.

Kincses WE, Braun C, Kaiser S, Elbert T. Modeling extended sources of event-related potentials using anatomical and physiological constraints. *Hum Brain Mapp* 8: 182–193, 1999.

Koechlin E, Hyafil A. Anterior prefrontal function and the limits of human decision-making. *Science* 318: 594–598, 2007.

Lachaux JP, Rodriguez E, Martinerie J, Varela FJ. Measuring phase synchrony in brain signals. *Hum Brain Mapp* 8: 194–208, 1999.

Lebedev MA, Nicolelis MA. Brain-machine interfaces: past, present and future. *Trends Neurosci* 29: 536–546, 2006.

Lebedev MA, Carmena JM, O'Doherty JE, Zacksenhouse M, Henriquez CS, Principe JC, Nicolelis MA. Cortical ensemble adaptation to represent velocity of an artificial actuator controlled by a brain-machine interface. *J Neurosci* 25: 4681–4693, 2005.

Levine SP, Huggins JE, BeMent SL, Kushwaha RK, Schuh LA, Passaro EA, Rohde MM, Ross DA. Identification of electrocorticogram patterns as the basis for a direct brain interface. *J Clin Neurophysiol* 16: 439–447, 1999.

Levine SP, Huggins JE, BeMent SL, Kushwaha RK, Schuh LA, Rohde MM, Passaro EA, Ross DA, Elisevich KV, Smith BJ. A direct brain interface based on event-related potentials. *IEEE Trans Rehabil Eng* 8: 180–185, 2000.

Millan Jdel R, Renkens F, Mourino J, Gerstner W. Noninvasive brain-actuated control of a mobile robot by human EEG. *IEEE Trans Biomed Eng* 51: 1026–1033, 2004.

Milner B, Corsi P, Leonard G. Frontal-lobe contribution to recency judgements. *Neuropsychologia* 29: 601–618, 1991.

Mormann F, Lehnertz K, David P, Elger CE. Mean phase coherence as a measure for phase synchronization and its application to the EEG of epilepsy patients. *Physica D* 144: 358–369, 2000.

Mosher JC, Leahy RM, Lewis PS. EEG and MEG: forward solutions for inverse methods. *IEEE Trans Biomed Eng* 46: 245–259, 1999.

Mulliken GH, Musallam S, Andersen RA. Decoding trajectories from posterior parietal cortex ensembles. *J Neurosci* 28: 12913–12926, 2008a.

Mulliken GH, Musallam S, Andersen RA. Forward estimation of movement state in posterior parietal cortex. *Proc Natl Acad Sci USA* 105: 8170–8177, 2008b.

Musallam S, Corneil BD, Greger B, Scherberger H, Andersen RA. Cognitive control signals for neural prosthetics. *Science* 305: 258–262, 2004.

Naghavi HR, Nyberg L. Common fronto-parietal activity in attention, memory, and consciousness: shared demands on integration? *Conscious Cogn* 14: 390–425, 2005.

Neal RM. *Bayesian Learning for Neural Networks*. New York: Springer, 1996, p. xi.

Newman SD, Carpenter PA, Varma S, Just MA. Frontal and parietal participation in problem solving in the Tower of London: fMRI and computational modeling of planning and high-level perception. *Neuropsychologia* 41: 1668–1682, 2003.

Norman DA, Shallice T. Attention to action: willed and automatic control of behavior. In: *Consciousness and Self-Regulation: Advances in Research and Theory*, edited by Davidson RJ, Schwarts GE, and Shapiro D. New York: Plenum: 1986, p. 1–18.

Onose G, Grozea C, Anghelescu A, Daia C, Sinescu CJ, Ciurea AV, Spircu T, Mirea A, Andone I, Spanu A, Popescu C, Mihaescu AS, Fazli S, Danoczy M, Popescu F. On the feasibility of using motor imagery EEG-based brain-computer interface in chronic tetraplegics for assistive robotic arm control: a clinical test and long-term post-trial follow-up. *Spinal Cord* 50: 599–608, 2012.

Perfetti B, Varanese S, Mercuri P, Mancino E, Saggino A, Onofrj M. Behavioural assessment of dysexecutive syndrome in Parkinson's disease without dementia: a comparison with other clinical executive tasks. *Parkinsonism Relat Disord* 16: 46–50, 2010.

Petrides M, Pandya DN. Dorsolateral prefrontal cortex: comparative cytoarchitectonic analysis in the human and the macaque brain and corticocortical connection patterns. *Eur J Neurosci* 11: 1011–1036, 1999.

Petrides M, Pandya DN. Efferent association pathways from the rostral prefrontal cortex in the macaque monkey. *J Neurosci* 27: 11573–11586, 2007.

Petrides M, Pandya DN. Efferent association pathways originating in the caudal prefrontal cortex in the macaque monkey. *J Comp Neurol* 498: 227–251, 2006.

Phillips C, Rugg MD, Friston KJ. Anatomically informed basis functions for EEG source localization: combining functional and anatomical constraints. *Neuroimage* 16: 678–695, 2002.

Phillips JW, Leahy RM, Mosher JC. MEG-based imaging of focal neuronal current sources. *IEEE Trans Med Imaging* 16: 338–348, 1997.

Pohlmeyer EA, Solla SA, Perreault EJ, Miller LE. Prediction of upper limb muscle activity from motor cortical discharge during reaching. *J Neural Eng* 4: 369–379, 2007.

Qin L, Ding L, He B. Motor imagery classification by means of source analysis for brain-computer interface applications. *J Neural Eng* 1: 135–141, 2004.

Ramnani N, Owen AM. Anterior prefrontal cortex: insights into function from anatomy and neuroimaging. *Nat Rev Neurosci* 5: 184–194, 2004.

Rivet B, Cecotti H, Phlypo R, Bertrand O, Maby E, Mattout J. EEG sensor selection by sparse spatial filtering in P300 speller brain-computer interface. *Conf Proc IEEE Eng Med Biol Soc* 2010: 5379–5382, 2010.

Roesch MR, Taylor AR, Schoenbaum G. Encoding of time-discounted rewards in orbitofrontal cortex is independent of value representation. *Neuron* 51: 509–520, 2006.

Rolls ET, Grabenhorst F. The orbitofrontal cortex and beyond: from affect to decision-making. *Prog Neurobiol* 86: 216–244, 2008.

Sarnrhein J, Petsche H, Rapperlsberger G, Shaw GL, von Stein A. Synchronization between prefrontal and posterior association cortex during human working memory. *Proc Natl Acad Sci USA* 95: 7092–7096, 1998.

Sarvas J. Basic mathematical and electromagnetic concepts of the biomagnetic inverse problem. *Phys Med Biol* 32: 11–22, 1987.

Sato MA. Online model selection based on the variational Bayes. *Neural Comput* 13: 1649–1681, 2010.

Schoenbaum G, Roesch MR, Stalnaker TA. Orbitofrontal cortex, decision-making and drug addiction. *Trends Neurosci* 29: 116–124, 2006.

Schoenbaum G, Takahashi Y, Liu TL, McDannald MA. Does the orbitofrontal cortex signal value? *Ann NY Acad Sci* 1239: 87–99, 2011.

Serruya MD, Hatsopoulos NG, Paninski L, Fellows MR, Donoghue JP. Instant neural control of a movement signal. *Nature* 416: 141–142, 2002.

Shan H, Yuan H, Zhu S, He B. EEG-based motor imagery classification accuracy improves with gradually increased channel number. *Conf Proc IEEE Eng Med Biol Soc* 2012: 1695–1698, 2012.

Shevade SK, Keerthi SS. A simple and efficient algorithm for gene selection using sparse logistic regression. *Bioinformatics* 19: 2246–2253, 2003.

Stam CJ, Nolte G, Daffertshofer A. Phase lag index: assessment of functional connectivity from multi channel EEG and MEG with diminished bias from common sources. *Hum Brain Mapp* 28: 1178–1193, 2007.

Taylor DM, Tillery SI, Schwartz AB. Direct cortical control of 3D neuroprosthetic devices. *Science* 296: 1829–1832, 2002.

Tomberg C, Desmedt JE. Human perceptual processing: inhibition of transient prefrontal-parietal 40 Hz binding at P300 onset documented in non-averaged cognitive brain potentials. *Neurosci Lett* 255: 163–166, 1998.

Torres EB. Signatures of movement variability anticipate hand speed according to levels of intent. *Behav Brain Funct* 9: 10, 2013.

Torres EB. Two classes of movements in motor control. *Exp Brain Res* 215: 269–283, 2011.

Torres EB, Zipser D. Reaching to grasp with a multi-jointed arm. I. Computational model. *J Neurophysiol* 88: 2355–2367, 2002.

Torres EB, Zipser D. Simultaneous control of hand displacements and rotations in orientation-matching experiments. *J Appl Physiol* 96: 1978–1987, 2004.

Torres EB, Heilman KM, Poizner H. Impaired endogenously evoked automated reaching in Parkinson's disease. *J Neurosci* 31: 17848–17863, 2011.

Torres EB, Quian Quiroga R, Cui H, Buneo CA. Neural correlates of learning and trajectory planning in the posterior parietal cortex. *Front Integr Neurosci* 7: 39, 2013.

Torres EB, Raymer A, Gonzalez Rothi LJ, Heilman KM, Poizner H. Sensory-spatial transformations in the left posterior parietal cortex may contribute to reach timing. *J Neurophysiol* 104: 2375–2388, 2010.

Vidal JJ. Toward direct brain-computer communication. *Annu Rev Biophys Bioeng* 2: 157–180, 1973.

Wallis JD, Miller EK. Neuronal activity in primate dorsolateral and orbital prefrontal cortex during performance of a reward preference task. *Eur J Neurosci* 18: 2069–2081, 2003.

Waszak F, Wascher E, Keller P, Koch I, Aschersleben G, Rosenbaum DA, Prinz W. Intention-based and stimulus-based mechanisms in action selection. *Exp Brain Res* 162: 346–356, 2005.

Weidner R, Krummenacher J, Reimann B, Muller HJ, Fink GR. Sources of top-down control in visual search. *J Cogn Neurosci* 21: 2100–2113, 2009.

Wessberg J, Stambaugh CR, Kralik JD, Beck PD, Laubach M, Chapin JK, Kim J, Biggs SJ, Srinivasan MA, Nicolelis MA. Real-time prediction of hand trajectory by ensembles of cortical neurons in primates. *Nature* 408: 361–365, 2000.

Wolpaw JR, McFarland DJ. Multichannel EEG-based brain-computer communication. *Electroencephalogr Clin Neurophysiol* 90: 444–449, 1994.

Wolpaw JR, Birbaumer N, McFarland DJ, Pfurtscheller G, Vaughan TM. Brain-computer interfaces for communication and control. *Clin Neurophysiol* 113: 767–791, 2002.

Wolpaw JR, McFarland DJ, Neat GW, Forneris CA. An EEG-based brain-computer interface for cursor control. *Electroencephalogr Clin Neurophysiol* 78: 252–259, 1991.

Yamada H, Nakatani T, Ebe K, Cichocki A, Choi K, inventors; RIKEN Brain Science Institute-Toyota Collaboration Center (BTCC). Mobile body control device and mobile control method. WIPO Patent WO 2010050113 A1, 2010.

Zhao Q, Zhang L, Cichocki A. EEG-based asynchronous BCI control of a car in 3D virtual reality environments. *Chin Sci Bull* 54: 78–87, 2009.